Proteomics of mouse brain endothelium uncovers dysregulation of vesicular transport pathways during aging

Katalin Todorov-Völgyi[1*+], Judit González-Gallego[1,2*], Stephan A Müller[3,4], Nathalie Beaufort[1], Rainer Malik[1], Martina Schifferer[3,5], Mihail Ivilinov Todorov[1,6], Dennis Crusius[1], Sophie Robinson[1,2,3], Andree Schmidt[3,4], Jakob Körbelin[7], Florence Bareyre[5,8,9], Ali Ertürk[1,5,6], Christian Haass[3,5,10], Mikael Simons[3,5], Dominik Paquet[1,5], Stefan F Lichtenthaler[3,4,5], Martin Dichgans[1,3,5+]

1) Institute for Stroke and Dementia Research (ISD), University Hospital, LMU Munich, Munich, Germany;
2) Graduate School of Systemic Neuroscience (GSN), University Hospital, LMU Munich, Munich, Germany;
3) German Center for Neurodegenerative Diseases (DZNE) Munich, Munich, Germany;
4) Neuroproteomics, School of Medicine and Health, Klinikum rechts der Isar, Technical University of Munich, Munich, Germany
5) Munich Cluster for Systems Neurology (SyNergy), Munich, Germany;
6) Institute for Tissue Engineering and Regenerative Medicine (iTERM), Helmholtz Zentrum München, Neuherberg, Germany;
7) Department of Oncology, Hematology and Bone Marrow Transplantation with Section Pneumology, University Medical Center Hamburg-Eppendorf, Hamburg, Germany;
8) Institute of Clinical Neuroimmunology, University Hospital, LMU Munich, Munich, Germany;
9) Biomedical Center Munich (BMC), Faculty of Medicine, LMU Munich, Planegg-Martinsried, Germany;
10) Biomedical Center (BMC), Division of Metabolic Biochemistry, Faculty of Medicine, Ludwig-Maximilians-Universität München, 81377 Munich, Germany.
* Contributed equally; + Correspondence

Electronic address:
Katalin.Voelgyi@med.uni-muenchen.de
Martin.Dichgans@med.uni-muenchen.de

Abstract

Age-related decline in brain endothelial cell (BEC) function critically contributes to neurological disease. Comprehensive atlases of the BEC transcriptome have become available but results from proteomic profiling are lacking. To gain insights into endothelial pathways affected by aging, we developed a magnetic-activated cell sorting (MACS)-based mouse BEC enrichment protocol compatible with proteomics and resolved the profiles of protein abundance changes during aging. Unsupervised cluster analysis revealed a segregation of age-related protein dynamics with biological functions including a downregulation of vesicle-mediated transport. We found a dysregulation of key regulators of endocytosis and receptor recycling (most prominently Arf6), macropinocytosis, and lysosomal degradation. In gene deletion and overexpression experiments, Arf6 affected endocytosis pathways in endothelial cells. Our approach uncovered changes not picked up by transcriptomic studies such as accumulation of vesicle cargo and receptor ligands including Apoe. Proteomic analysis of BECs from Apoe deficient mice revealed a signature of accelerated aging. Our findings provide a resource for analysing BEC function during aging.

Introduction

The central nervous system requires a tightly controlled metabolic environment for proper neuronal functioning and information processing. This specific environment is maintained by the blood-brain barrier (BBB), which is centrally positioned within the neurovascular unit and endowed with unique properties[1]. Brain endothelial cells (BECs), key constituents of the BBB, display exquisitely low rates of transcellular vesicular transport (transcytosis) and specialized tight junctions (TJs) that restrict paracellular diffusion thus safeguarding BBB integrity[2]. BECs further play critical roles in neurovascular coupling[3,4], brain metabolism[5], and immune activation[6] through interaction with other cells.

Age-related dysregulation of BECs causes vascular dysfunction thus critically contributing to cerebrovascular and neurodegenerative diseases[7-12]. Previous studies have shown a decline of various BEC-dependent functions during aging including BBB integrity[13,14], neurovascular coupling[15], and cerebral blood flow[16]. However, the molecular alterations driving this decline are insufficiently understood. Candidate factors that have emerged from prior work include an increase in oxidative and nitrosative stress[17,18], changes in telomere length resulting in cellular senescence[19] and specific molecules such as integrins[20,21], ApoE[22,23] and Medin, an amyloidogenic peptide that accumulates in the vasculature with aging[24-26].

Molecular profiling studies have greatly contributed to understanding the effects of aging on specific tissues or cell types[27-29]. Specifically, single-cell RNA sequencing (scRNAseq) of mouse BECs, along with proteomics of whole brain microvasculature have shown an aged-dependent shift in BBB transcytosis from ligand-specific receptor-mediated transport to non-specific caveolar endocytosis[30]. scRNAseq studies further revealed zonation-dependent transcriptomic changes in aged BECs[31,32] and an upregulation of innate immunity and oxidative stress response pathways in capillary BECs from old compared to young mice[31].

While developments in transcriptomic analyses have enabled cellular mapping at single cell resolution[33], analyses of the proteome are needed for better understanding of the molecular pathways implicated in cellular function and aging. First, correlations between mRNA levels and their corresponding protein

levels are often poor (Pearson´s r^2 0.3-0.4)[34-38], because posttranscriptional processes that control protein synthesis and degradation have a major influence on protein abundances. Second, transcriptomic analyses typically do not capture molecules that are bound to the cell surface or internalized such as receptor ligands or cargo from phagocytotic vesicles, respectively. Third, proteins are closer to the biosynthetic output and cellular functions than mRNA, however, to the best of our knowledge, results of BEC proteomic profiling are lacking.

Here, we developed a BEC enrichment protocol compatible with liquid chromatography coupled tandem mass spectrometry (LC-MS/MS) to resolve the mouse BEC proteome and gain insights into protein abundance changes during healthy aging. Using a recently developed method for unsupervised clustering[39-42] we identified distinct patterns of age-related protein dynamics that segregated with biological functions and the subcellular localization of proteins. We provide insights into endothelial vesicular transport pathways and identify Arf6, a key regulator of endocytosis and receptor recycling, as a candidate factor mediating vesicular transport changes during aging. We further present evidence for an accelerating effect of Apoe deficiency on BEC aging as well as cell autonomous effects of APOE in human endothelial cells.

Results

Proteomic analysis of mouse BECs during aging

To assess changes of the mouse BEC proteome during aging we first developed a protocol for BEC enrichment compatible with LC-MS/MS (**Fig. 1a**). Cd31-labeling and MACS resulted in the enrichment of BECs expressing adherens (Pecam1, Cdh5) and tight junction markers (Cldn5) (**Fig. 1b**). Isolated BECs from 3 and 18-months-old animals displayed ultrastructural hallmarks of endothelial cells including nuclei with heterochromatin and endothelial protrusions[43] (**Fig. 1b**). LC-MS/MS on isolated BECs and full brain tissue (FT) preparations from 3-months-old mice followed by label-free quantification (LFQ) showed a massive enrichment of endothelial markers including Nos3 (FC: 1684.5), Cdh5 (29.9), and Pecam1 (30.7) in BECs compared to FT (**Fig. 1c, Suppl. Table 1**). Notably, their protein levels in BECs were stable between 3 and 18 months. Among other cell markers we found a prominent reduction of neuronal (Map2 – FC: 0.01) and glial markers (Gfap – FC: 0.28), a moderate reduction of glial end-feet markers (Aqp4 – FC: 0.77), and some enrichment of pericyte (Anpep – FC: 4.82) marker proteins. This is consistent with the results of CD31-based enrichment protocols for single-cell sequencing[44], showing that a small population of other vascular cell types remains with these protocols.

Proteomic analysis of isolated BECs from 3, 6, 12, and 18-months-old mice captured a total of 4137 proteins. Among them, 3754 proteins were identified with ≥ 2 unique peptides of which 2516 proteins were quantified in ≥ 3 samples in all age groups. 850 proteins showed significant changes in abundance during aging (ANOVA, p-value < 0.05) (**Fig. 1d, Suppl. Table 2**). A comparison with published mouse bulk BEC RNA-seq data[45] revealed 193 proteins and corresponding RNAs that were significantly altered in both datasets (**Fig. 1e**). Notably, there was a weak but significant correlation (r^2=0.154; p<0.0001) between the log2 fold change values of the significantly altered BEC proteins and corresponding RNAs when comparing aged (18 and 19 months, respectively) to young (3-months-old) mice (**Fig. 1e**). Using 3-months-old animals as a reference, there was a steady increase in the number of significantly altered proteins from 3 (6 months) to 57 (12 months) to 339 proteins (18 months) (FDR p-value < 0.05) (**Fig. 1f, Suppl. Table 2**) consistent with previous bulk RNA-seq studies on whole organs and

BECs that found a large number of differentially regulated genes in old compared to young mice [45,46]. Unexpectedly several neurofilament (Nefm, Nefl, Ina) and myelin sheet (Mog, Mbp, Plp1) proteins while being strongly depleted in BECs compared to FT (**Fig. 1f,** right panel) were upregulated in the BEC proteome during aging (**Fig. 1f**, volcano plots). Immunolabeling and electron microscopy analysis of isolated BECs and brain capillaries confirmed the endothelial localization of Mbp and the engulfment of multilamellar membranous structures by aged endothelium, respectively (**Fig. 1g**). These results are in line with recent findings showing that microvascular endothelial cells act as 'amateur' phagocytes to engulf myelin debris[47] and contribute to the degradation of neurofilaments during aging[48,49].

Age-related protein expression dynamics

Genes with similar expression dynamics have been shown to share biological functions[50]. To characterize the temporal profile of age-related BEC protein levels in greater detail, we first clustered all identified proteins based on their abundance patterns across time points (3, 6, 12 and 18 months of age). Unsupervised clustering using Bayesian nonparametric time-series modeling revealed 16 clusters that varied in size between 44 and 312 identified and 6 to 119 significantly altered proteins (**Fig. 2a**). Notably, several of the most abundant clusters showed opposing trends in their abundance dynamics during aging (**Fig. 2b, Extended Data. Fig. 1**). To identify possible links between BEC protein dynamics and function, we categorized significantly altered proteins in each cluster according to their subcellular localization (SL) and biological processes (BP) using Gene Ontology (GO) terms. As illustrated by Clusters 1 to 4 there was a segregation of clusters with individual GO terms and an alignment between SLs and corresponding BPs (**Fig. 2a**).

Focusing on significantly enriched biological processes we found a more than 5-fold enrichment of proteins related to *translation* (e.g. Rpl and Rps) in cluster 9, which was characterized by temporary downregulation at 12 months of age (**Fig. 2a-c**). *RNA-splicing* related proteins (e.g. Srsf) were enriched in cluster 3 showing a continuous downregulation until 18 months of age. In contrast, proteins related to *oxidation-reduction* (e.g. Prdx5) and *lipid metabolism* (e.g. Fasn) were enriched in cluster 4, which exhibited significant upregulation at 18 months of

age. Proteins related to *cytoskeleton organization* (e.g. Vcl and Pxn), and *cell adhesion* (e.g. Ctnnd1 and Tjp1/2) were enriched in cluster 2 showing temporary downregulation at 6 months of age. *Vesicle-mediated transport* proteins (e.g. Arf6 and Tmed2) were enriched in cluster 3 and showed a continuous downregulation during aging (**Fig. 2a-c**) while the *vesicle / exosome* subcellular localization was represented in multiple clusters with vastly different profiles (**Fig. 2a**). Collectively, these findings demonstrate close links between age-related protein abundance dynamics and individual biological processes including vesicle-mediated transport pathways.

BEC proteins implicated in endothelial vesicular transport

Given the central role of BECs in maintaining BBB integrity and recent data showing an age-related shift from ligand-specific receptor-mediated to non-specific caveolar transcytosis[30], we next turned to vesicle-mediated transport proteins and transmembrane receptors (**Fig. 3a, Suppl. Table 2**).

Focusing on vesicle-related proteins, we found major regulators of macropinocytosis (Rhog), dynamin-mediated endocytosis (Dnm1), exocytosis (Rab3a), multivesicular body formation (Ptpn23) and lysosomal degradation (Scarb2 and Ctsd) to be upregulated with aging, whereas the main vesicle-coating proteins (Arf6, Clta/c, and Cav1) were downregulated (**Fig. 3a**). Out of the 20 exocytosis-related proteins 16 proteins were positive regulators of exocytosis and showed increased protein abundance, suggesting an increased level of exocytosis during endothelial aging (**Suppl. Table 2**). Endothelial nitric oxide synthase (Nos3) a regulator of caveolin-mediated endocytosis[51] was transiently downregulated. ER-Golgi vesicle-mediated transport encompassed proteins that were upregulated (Mia, Uso1, and Vti1b) and downregulated (Tmed2, Tmed7) with aging, as were regulators of clathrin-mediated endocytosis (upregulated: Pacsin1, Hip1r, Aak1, and Ap2a1; downregulated: Dab2, Ap2a, and Arf6).

Focusing on endothelial receptors, we found that multiple subunits (Itga3/7/v and Itgb3/4/8) and ligands (Mfge8, Lamc1, and Fga/Fgg) of the integrin receptor complex were upregulated with aging, while transferrin receptor (Tfrc), the Itga1 receptor subunit and Lama5 ligand exhibited an aged-related transient downregulation (**Fig. 3a**). To further check, whether the reduction in Tfrc levels is

due to an age-related increase in receptor shedding, we performed single tryptic peptide analysis at 18 versus 3 months of age. In total, we found 2 and 13 peptides from the intra- and extracellular regions, respectively, to be significantly downregulated to a comparable extend in aged BECs, arguing against altered Tfrc shedding (**Extended Data. Fig. 2**). The tight junction scaffolding proteins Tjp1 and 2 and the adherent junction protein Ctnnd were likewise downregulated during aging.

We next explored the specificity of age-related protein changes of vesicle-mediated transport in BECs compared to the whole brain vasculature (BV) and found no correlation between the two preparations (**Fig. 3b, Suppl. Table 3**). Specifically, Arf6, Tfrc, Tmed2, Cav1, Rhog, and Scarb2, which were among the most significantly dysregulated proteins in BECs were not significantly altered in BV during aging. In contrast, Mfge8 (Milk fat globule-EGF factor-8 or Lactadherin) and Apoe were significantly upregulated in both BEC and brain vessel preparations (**Fig. 3c-d**), consistent with their role as ligands of the integrin receptor complex.

The most significantly downregulated protein in BECs was Arf6 (ANOVA, FDR q-value = 0,002), a key regulator of clathrin-dependent, caveolin-dependent, and clathrin and caveolae-independent endocytosis, as well as vesicle-mediated recycling of transmembrane receptors and junction proteins[52,53] (**Fig. 3a**).

To validate the age-related reduction of Arf6 levels, we performed immunocytochemistry on isolated BECs prepared from aged (18-months-old) and young (3-months-old) mice. Co-staining for Arf6 and Tfrc along with Pecam1 confirmed their BEC-specific reduction during aging with some evidence for a shift in the cellular distribution of Tfrc in isolated aged BECs (**Fig. 3e**). In contrast, immunocytochemical analysis of isolated brain parenchymal vessels for Arf6 and Tfrc along with ColIV showed no significant age-related alteration (**Fig. 3e**), which however agrees with the vessel proteomics data (**Fig. 3d**).

These findings emphasize the importance of cell type-specific proteomics for studying vesicular transport mechanisms during aging. They further highlight the candidacy of Arf6 in mediating age-related protein changes of endothelial vesicle-mediated transport and the recycling of transmembrane receptors.

Endothelial Arf6 and vesicle-mediated transport pathways

To better understand the role of Arf6 in BECs we conducted gene deletion and overexpression experiments. We first performed proteomic analyses in mice with EC-specific Arf6 deficiency and in human iECs derived from ARF6-KO iPSCs (**Fig. 4a** and **e top, Extended Data Fig. 3** and **4**). We found a 30% reduction of Arf6 levels in EC-Arf6-KO BECs, whereas Arf6 was not detected in Arf6-KO iPSCs (**Fig. 4b** and **f**). 312 and 1724 proteins were significantly altered in BECs and iECs, respectively (**Suppl. Table 4** and **6**). Enrichment analyses of significantly downregulated proteins showed mRNA processing and splicing to be among the most affected biological processes in both models (**Fig. 4c** and **g**) consistent with our findings on the aged BEC proteome (**Fig. 2**). Moreover, chromatin remodeling and nucleosome assembly related proteins were likewise downregulated in mouse and human, respectively, in line with the previously published role of Arf6 in cell division[54].

Focusing on vesicle-mediated transport proteins we found a similar proportion of proteins being up- and downregulated upon Arf6 deletion in mice (**Fig. 4b** and **d**) whereas in ARF6 deficient iECs there was an overrepresentation of upregulated proteins (120 out of the 184 vesicle-mediated transport proteins (**Fig. 4f** and **h**). We therefore performed functional experiments in ARF6-KO iECs and found an increased level of endocytosis (FM1-43FX in newly formed vesicles). This upregulation of endocytosis despite Arf6 deletion potentially reflecting a compensatory response (**Fig. 4j**).

To further investigate consequences of Arf6 modulation we performed overexpression experiments by infecting mice with BEC specific[55] Arf6-GFP-AAV or GFP-AAV (used as control) followed by BEC proteomics (**Fig. 4a**, bottom, **Suppl. Table 5**). To validate the specificity of the virus and the efficiency of virus transduction, we performed immunohistochemistry on the olfactory bulb region of GFP-AAV-treated mice and found that 45% of the CD31-labeled vasculature were GFP positive (**Fig. 4i**). Proteomic analysis confirmed a 1.7-fold increase of Arf6 levels in BECs (**Fig. 4k**). Enrichment analysis of significantly upregulated proteins revealed vesicle-mediated transport, activation of GTPase activity, and ER to Golgi vesicle-mediated transport to be among the most significantly affected biological processes (**Fig. 4k** and **m**). Aside from the small GTPase Arf6, both the small GTPase binding-protein Gga2, and the small GTPase activating

protein Tbc1d20 were upregulated. The most significantly downregulated protein was Glb1, a marker of cellular senescence and ageing (**Fig. 4k**).

ARF6-overexpression in iECs was done with Arf6-GFP-AAV vs GFP-AAV treatment and resulted in a 1.9-fold increase of ARF6 levels (**Fig. 4e**, bottom, **Fig. 4n** and **p, Suppl. Table 6**). As in Arf6-GFP-AAV treated mice, enrichment analysis of significantly upregulated proteins revealed vesicle-mediated transport related GO terms to be among the most prominently affected biological processes (**Fig. 4n** and **o**). Specifically, ARF6 and its binding-protein GGA2, DNM1L and the Conserved oligomeric Golgi complex (COG) subunit COG5 were upregulated in both mouse and human (**Fig. m** and **p**). In fact, several subunits of COG were among the most prominently upregulated proteins in iECs (**Fig. 4p**).

Apoe-deficiency results in a signature of accelerated BEC aging

To explore potential relationships between age-related BEC proteome changes and human brain disorders, we next applied over-representation analysis (ORA) on disease-related databases. Focusing on BEC proteins that were altered during aging (ANOVA p-value < 0,05) we found an overrepresentation (FDR, p-value < 0,05) of disease terms related to neurodegenerative disease (8 of the top 25 disorders, highlighted in grey in **Fig. 5a**). Among these terms were Alzheimer's disease (AD), Parkinson's disease (PD), and Vascular dementia (VaD), which have previously been related to vascular or endothelial processes[56-58]. Hence, we focused on these conditions. Overall, we found 30 AD (23 up, 7 down), 34 PD (18 up, 16 down) and 9 VaD (5 up, 4 down) -associated proteins to be significantly dysregulated during aging (**Fig. 5b**). While the disease-related association does not imply that these proteins are directly causative of neurodegenerative diseases, many of them are known risk genes for AD, PD or VaD (eg. App, Snca or Apoe). Apoe and Tomm40, which were up- and downregulated in BECs during aging, respectively, were associated with all three conditions (**Fig. 5b**). Given the widely recognized role of Apoe in brain cellular aging[59-62], and of Apoe deficiency in causing endothelial dysfunction[63-65], we next compared the BEC proteomes of young (3-months-old) Apoe-KO and WT mice (**Suppl. Table 7**). Using proteomics, 111 and 103 proteins were significantly (p-value < 0,05) up- and downregulated, respectively, in Apoe-KO mice (**Fig. 5c**). Comparing the BEC proteomic signature of young Apoe-KO mice with the signature of aged (18-

months-old) WT mice we found a positive correlation (r=0.769; r^2=0.501, p<0.0001) suggesting an accelerating effect of Apoe deficiency on BEC aging. Notably, Arf6 was significantly downregulated in young Apoe-KO mice (fold-change: 0.58) (**Fig. 5d**). Directionally consistent changes in young Apoe-KO and aged WT mice were further seen for several other proteins implicated in endothelial vesicle-mediated transport (**Fig. 5d-e**).

Focusing on the Arf6-Apoe interaction network in aged mice we found 19 and 24 significantly altered proteins at 18 compared to 3 months of age to exhibit direct experimentally determined connections with Arf6 and Apoe, respectively (**Fig. 5f**, for details see methods). The vesicular transport protein Tgoln1 (Trans-Golgi network integral membrane protein 1) showed a direct relationship with both Arf6 and Apoe. Notably, Mfge8 and Apoe showed multiple shared connections as did Arf6 and Tfrc. Also, the integrin (Itgav/b3) receptor ligands Mfge8, Lamc1, and Fga/Fgg all had a direct connection with Apoe and Tgoln1.

Among the AD-related proteins, we found App (Amyloid beta precursor protein) to be upregulated during BEC aging at 12 versus 3 months of age. In addition, the App processing proteins Itm2b (Integral membrane protein 2B) and Htra2 (Serine protease HTRA2, mitochondrial) were likewise upregulated with BEC aging (**Fig. 5b**).

Some of the documented effects of Apoe deficiency on endothelial cells are mediated through systemic effects in Apoe-KO mice including hyperlipidemia[63,64]. To identify cell-autonomous effects of APOE in endothelial cells, we next applied genome editing in human iPSCs to obtain a human APOE-KO line and differentiated these cells into iECs (**Fig. 5g-h, Extended Data Fig. 5-6**). Proteomic analysis revealed 326 significantly altered proteins between APOE-KO and WT iECs (**Fig. 5i, Suppl. Table 8**). Enrichment analysis of significantly downregulated proteins showed vesicle-mediated transport and vesicle fusion to be among the most significantly affected biological processes (**Fig. 5j**). Specifically, among the 28 significantly altered vesicle-mediated transport proteins 23 were downregulated (**Fig. 5k**). Accordingly, we found reduced levels of endocytosis of FM1-43FX in newly formed vesicles in APOE-KO iECs (**Fig. 5l**). Collectively, our *in vivo* findings highlight the relevance of age-related BEC proteome changes for human disease and a signature of accelerated BEC aging in 3 months old Apoe-KO mice. They further suggest cell-autonomous effects of

APOE in human endothelial cells. However, a more comprehensive understanding of EC-autonomous regulation by Apoe would require further experiments.

Discussion

Using a mass spectrometry compatible protocol for BEC enrichment, we provide an unbiased characterization of the mouse BEC proteome during aging. Unsupervised clustering revealed distinct patterns of age-related protein expression dynamics that segregated with biological functions and subcellular localizations. We provide insights into endothelial pathways of vesicular transport highlighting key regulators (e.g. Arf6), ligands, and cargos. We also present evidence for an accelerating effect of Apoe deficiency on BEC aging and a cell autonomous role of APOE in human ECs. We further offer a publicly available resource and searchable database of age-related protein dynamics of mouse BECs (available at http://becaging.de) for wider use.

Among the most prominent changes was a decline in the abundancy of proteins implicated in vesicle-mediated transport. Several observations point to a possible role of Arf6, the most significantly downregulated protein in our dataset, in mediating these changes. First, Arf6, a small GTPase, is a key regulator of membrane trafficking, endocytosis, and vesicle-mediated recycling of transmembrane receptors and junction proteins[52,66,67]. Second, Arf6 was coregulated with proteins implicated in clathrin-mediated endocytosis (Cltc and Dab2)[68], vesicular transport from ER to Golgi (Arf4, Tmed2, and Tmed7) and receptor recycling (Rab5c and Vps26b), all of which were continuously downregulated with aging. Third, downregulation was further seen for Cav1 lipid raft protein, which together with Arf6 is implicated in caveolin-mediated endocytosis[66], and further regulates the expression of Tjp1[69]. Experiments in CHO cells transfected with a dominant negative Arf6 mutant have shown a redistribution of Tfrc from the cell surface to vesicles and reduced receptor recycling[68]. In accordance with this, we found a similar redistribution of Tfrc in isolated BECs from aged mice (**Fig. 3E).** However, additional experiments would be needed to consolidate this observation. Of note, while Arf6 was prominently reduced in aged BECs, it was not changed in isolated brain vessels during aging. As Arf6 is expressed by multiple cell types in the brain and since brain vessel preparations contain pericytes, glial- and synaptic endings in addition to endothelial cells, the lack of a decrease in Arf6 levels in the aged vessel preparation might relate to the overall pattern of Arf6 expression in non-

endothelial vascular cell-types. Further experiments would be needed, to explore the cell specific expression pattern of Arf6 during aging.

To explore the regulatory function of Arf6 on mouse and human endothelial cells we next performed Arf6 deficiency and overexpression experiments. In unbiased bioinformatic analyses we found mRNA-processing among the most prominently downregulated biological processes upon endothelial Arf6 deficiency in both mouse and human, consistent with our aged BEC proteomics data. Proteins related to vesicle-mediated transport were mostly upregulated in ARF6-KO iECs in accord with an increased level of endocytosis detected by FM1-42FX experiments (**Fig. 3** and **Fig. 4**). As a limitation of our Arf6-deficient mouse model, the reduction of Arf6 levels in our BEC preparations was only 30%. This moderate reduction might be due to (i) incomplete recombination efficiency after tamoxifen induction, (ii) some contamination by non-endothelial Arf6-expressing cell types during MACS-based enrichment[44], or (iii) endothelial endocytic uptake of Arf6-containing extracellular vesicles produced by other cell types other cell types[70,71]. Overexpression of Arf6 resulted in vesicle-mediated transport being among the most affected upregulated processes in both mouse and human endothelial cells. In particular, we found proteins involved in GTPase activity to be upregulated in mouse BECs, suggesting an increased activity of Arf6 small GTPase in Arf6-AAV-treated animals. Subunits of the COG complex were upregulated in human iECs, suggesting a positive regulation in the maintenance of intra-Golgi trafficking[72]. Glb1, a marker of cellular senescence[73,74] was among the most prominently downregulated proteins in Arf6-AAV treated mice with an opposite pattern in mice with endothelial Arf6 deficiency. These data align well with the prominent downregulation of Arf6 in aged BECs, further highlighting the importance of Arf6 during aging (**Fig. 3** and **Fig. 4**).

In contrast to Arf6-related vesicular pathways, some of the major regulators of micropinocytosis (Rhog), multivesicular body formation (Ptpn23), and lysosomal degradation (Scarb2) were upregulated (**Fig. 3a**) consistent with an activation of protein degradation during aging[75]. We further found constituents of both myelin (e.g. Mbp, Mog, Plp1) and axons (e.g. Nefl, Nefm, Ina) to accumulate in aged BECs consistent with the previously reported role of BECs in clearing myelin debris after spinal cord injury and experimental autoimmune encephalitis[47,76]. Interestingly, Scarb2, a regulator of lysosomal/endosomal transport, and Ppt1, a

glycoprotein involved in lysosomal degradation were likewise upregulated during aging. However, whether this relates to the degradation of myelin debris remains unknown.

Our results complement and extend RNAseq studies on BECs during aging. Specifically, and in accordance with recent scRNAseq data[30,45], we found an age-dependent downregulation of the receptor-mediated endocytosis components Tfrc, Cltc, Clta, and Dab2 although Cav1, which is implicated in receptor-independent transcytosis, was likewise downregulated during BEC aging. Tfrc is the most widely studied and validated target protein for receptor-mediated transcytosis-based delivery approaches[77,78]. Indeed, some approaches have shown promising results in clinical trials[79]. Tfrc-based strategies receive growing interest for delivering therapeutics in age-related neurodegenerative diseases including AD[80]. The observed downregulation of Tfrc in aged mice suggest that these strategies might be less effective in aged organisms.

Our proteomics approach further captured processes that were not detected at RNA level. Specifically, we found changes in the abundance of ligands and cargo (e.g. of myelin proteins) originating from other cellular sources. In principle, the increased levels of ligand and cargo proteins can be due to an increase in cargo availability, an increase in endothelial phagocytosis (as suggested by upregulated Mfge8 or Apoe opsonin proteins), or a decrease in cargo digestion. Several receptor-ligand pairs including the Mfge8, Lamc1, and Fgg/Fga ligands and the integrin receptor subunits Itga3/7/v and Itgb3/4/8 were upregulated with aging (**Fig. 2a**). Integrins are heterodimeric transmembrane proteins composed of alpha and beta subunits occurring in multiple combinations[81]. We found most of the subunits to be upregulated with aging whereas Itga1 and its ligand Lama5 were both downregulated. Fibrinogen (represented with Fgg and Fga), a blood-born protein that is synthesized by the liver, accumulated with aging possibly through interaction with its receptor Itgavb3[82], which was likewise upregulated. In principle, this might reflect altered fibrinogen-binding, intracellular uptake, or extravasation.

Among the proteins that were continuously upregulated with aging was Mfge8, which is best known for its role in phagocytosis of apoptotic cells but also implicated in neovascularization[83] and vascular amyloidosis[25,84]. In the vasculature, Mfge8 is primarily expressed by mural cells and astrocytes[85]. Mfge8-

mediated clearance of apoptotic cells is mediated via integrin receptors on phagocytosing cells (specifically Itgavb3 or Itgavb5)[83,86] and we found Mfge8 and Itgavb3 to be coregulated in BECs during aging (cluster 1). However, whether this relates to the clearance function of BECs remains to be investigated.

Our over-representation analysis on disease-related databases revealed a significant enrichment of proteins associated with neurodegenerative diseases, while also highlighting Apoe, which is known to be involved in lipid metabolism, mitochondrial function, and immunoregulation[87]. In the brain vasculature Apoe is primarily expressed by microglia and astrocytes[85] and to a lesser extent by other cells including BECs[85,88]. Hence, the elevated endothelial level of Apoe protein during aging might reflect its endothelial accumulation as a ligand rather than changes in production or secretion by endothelial cells. There is a broad literature on individual Apoe genotypes and cerebrovascular dysfunction highlighting a role of pericytes[23] and also BECs[89] in mediating the effects of APOE4 on BBB function primarily through non-cell-autonomous mechanisms. Our proteomic results in 3-months-old Apoe-KO mice revealed a profile of accelerated BEC aging with several proteins involved in vesicular transport. Protein network analysis further revealed direct connections of Apoe with the Tgoln1 trans-Golgi network protein, and multiple integrin receptor ligands, including Mfge8, Lamc1 and Fgg/a. These changes might in part relate to non-cell-autonomous mechanisms including effects related to hyperlipidemia[63,64]. However, proteomic and functional measurements of APOE-KO human iECs revealed a downregulation of vesicle-mediated transport and vesicle fusion related proteins with decreased level of endocytosis, suggesting a cell autonomous effect of APOE on endothelial vesicular transport.

Additional changes with BEC aging in terms of biological processes were an overall decline of RNA-splicing (cluster 3) and translation (cluster 9). We further found an increase in oxidation-reduction (cluster 4) consistent with previous literature showing enhanced oxidative stress during cerebrovascular aging [90-92]. Unsupervised clustering revealed a co-regulation of proteins implicated in cell adhesion and cytoskeleton organization with a prominent reduction at 6 months of age (cluster 2). Among them were multiple components of the adherent junction forming complex (Cdh5, Ctnna1, Ctnnb1, Ctnnd1/p120) and its connecting actin-filament binding proteins (Vcl and Pxn)[93]. Ctnnd1/p120

regulates the degradation of Cdh5 via clathrin-mediated endocytosis[94], which was likewise downregulated during aging. The interaction between Ctnnd1/p120 and Cdh5 is required for maintenance of endothelial barrier function[95]. Whether BBB integrity is compromised during normal aging is still controversial[14]. However, we found the expression levels of the tight junction proteins Tjp1 and Tjp2, major regulators of vascular permeability[96,97] to be likewise downregulated. As a limitation, we could not combine fluorescence-activated cell sorting (FACS)-based isolation of BECs with LC-MS/MS-based proteomics as this would have required pooling brain samples from multiple animals thus loosing information from individual mice (e.g. protein changes which are detectable only in individual samples) and reducing statistical power[98]. Second, in contrast to single cell RNA sequencing (scRNAseq) approaches our technique does not allow differentiating between BEC subtypes and addressing vascular zonation-specific aspects. Third, differentiation protocols of iPSCs into endothelial cells do not fully recapitulate endothelial functions and have not been well established to differentiate organ-specific endothelial cell subtypes. Furthermore, iPSC-derived endothelial cells may not completely resemble primary endothelial cell functionality *in vivo*[99]. Fourth, our protocol did not enable parallel investigation of the mouse BEC transcriptome from the same BEC preparations as the BEC sample purification protocol is different for transcriptomics and proteomics. Still, we integrated data from previous scRNAseq studies on BEC aging offering further insights, and also compared the age-related proteome changes of BECs with BVs to explore the cell specificity of the detected vesicular transport protein changes. Fifth, the mouse BEC and human iEC proteomes (concentration detection range 3-4 and 4-6 orders of magnitude, respectively) represent an incomplete snapshot of proteins. Future improvements in LC-MS/MS technology may enable quantification of very low abundant proteins, such as transcription factors or specific signaling molecules. As a final limitation, age-related changes in murine BECs may differ from those in humans, which, however, are difficult to assess as the isolation protocol requires freshly dissected brain tissue.

In summary, we resolved the mouse BEC proteome during aging and identified distinct patterns of age-related expression dynamics that segregated with biological functions and the subcellular localization of proteins. We provide insights into endothelial vesicular pathways highlighting key regulators, ligands,

517 and cargo, and present evidence for an accelerating effect of Apoe deficiency on
518 BEC aging. Our findings further imply a cell autonomous role of APOE in human
519 endothelial cells. Altogether, this study provides a framework for understanding
520 key endothelial pathways during aging and serves as a resource for analyses of
521 BEC function.

Materials and methods

Animals

Animal experiments were performed in accordance with the German Animal Welfare Law (§4 TschG) and approved by the Government of Upper Bavaria (Vet_02-21-139). For all of our animal experiments we used mixed gender groups in the same ratio of male and female mice in the range of 20-30g body weight up to 18 months of age. Animals were kept under standard conditions in a specific pathogen-free facility at 20-24°C and 45-65% humidity on a 12-h light/dark cycle and had access to food and water ad libitum.

Brain specimens were obtained from C57BL/6J mice at 3, 6, 12, and 18 month of age (Charles River Laboratories, Germany), 3-months-old C57BL/6J Apoe-/- mice, and 3-months-old Arf6fl/fl;Cdh5(CreERT2) mice.

To enable comparisons of age-related proteomic changes with published transcriptomic datasets, age groups were selected based on the publicly available mouse maturation rate (The Jackson Laboratory, https://www.jax.org/news-and-insights/jax-blog/2017/november/when-are-mice-considered-old) and BEC transcriptomics datasets93-96 (see Fig. 1E) as follows: (1) Beginning of mature adult phase (3 months of age), (2) end of mature adult phase (6 months of age), 3) middle-aged phase (12 months of age), (4) beginning of old phase (18 months of age).

$Arf6^{fl/fl}$;Cdh5(CreERT2) mice were obtained by crossing B6.Cg-Arf6tm1.1Gdp/J mice (Jackson 028669[100]) with Tg(Cdh5-cre/ERT2)1Rha mice (a kind gift from Ralf H Adams, London Research Institute[101]). Arf6 deletion was induced by 3 intraperitoneal tamoxifen injections (each 0,25 mg/g KGW, dissolved in Miglyol 812) in 2-month-old $Arf6^{fl/fl}$, $Cre^{+/-}$ mice. $Arf6^{fl/fl}$, $Cre^{-/-}$ mice treated with tamoxifen served as negative control. Animals were terminated at 3 months of age.

Mice were aged in the animal facility of the Institute for Stroke and Dementia Research and housed in isolated ventilated HEPA filtered cages (12 h light/dark cycle with *ad libitum* access to food and water). Tissues were harvested in parallel and during the same daytime.

Proteomic and immunocytochemical experiments were done on n=4-8 mice per group, except proteomic analysis of BECs from AAV-treated mice which was

performed on 4 independent BEC isolates derived from n=2 C57BL6J mice per group.

Tissue harvesting

For BEC isolation, mice were deeply anesthetized using ketamine (100 mg/kg, i.p) -xylazine (10 mg/kg i.p), and transcardially perfused with ice-cold 20 ml 1X Hank's Balanced Salt Solution (HBSS) and dissected. Following perfusion, the brain was surgically removed and kept in HBSS at 4 ºC for further analysis.

For immunohistochemical analysis, anesthetized animals were perfused with 1X HBSS and transcardially fixed with 4 % paraformaldehyde (PFA). The dissected brain samples were incubated overnight in 4 % PFA for vibratome sectioning.

For vessel isolation, anesthetized animals were perfused with 1 X PBS and the dissected brains immediately frozen on dry ice and stored at -80 ºC until use.

Brain endothelial cell isolation (BECs)

The entire brain without the olfactory bulb was used for BEC isolation. First, the brain was transferred to a Petri Dish placed on ice and minced with a scalpel. BECs were isolated using a modified version of the Adult Brain Dissociation kit (Miltenyi Biotec, Cat# 130-107-677), which allows for mechanical and enzymatic tissue dissociation. After tissue homogenization and filtration through 70 µm cell strainers (Corning, Cat# 431751), myelin was removed using a 30 % Percoll gradient (GE Healthcare Cat# 17-5445-02) followed by removal of erythrocytes using the Red Blood Cell Removal Solution (Miltenyi Biotec, Cat# 130-094-183). BECs were enriched from the single cell suspension using CD31 MicroBeads (Miltenyi Biotec, Cat# 130-097-418) and magnetic activated cell sorting (MACS) using a modified MACS buffer with low bovine serum albumin (BSA) content (L-MACS buffer; containing 0.25 % BSA (BSA Fraction V, Sigma-Aldrich, Cat#10735096001) and 2 mM EDTA (ThermoFisher, Cat# 15575020) in PBS with calcium and magnesium (Corning, Cat#21-030-CV)). Following CD31 enrichment, the cell suspension was washed twice with PBS to remove residual L-MACS buffer and subsequently pelleted cells were used for further protein extraction.

Brain vessel isolation (BV)

Brain vessels were isolated from whole cerebrum as described previously[102,103]. Brain tissue was placed on ice, minced with a scalpel, and homogenized in 15 mL of cold minimum essential medium (ThermoFisher, Cat# 11095080) using a glass tissue grinder (Wheaton). After dissociation, myelin was removed using a 15 % Ficoll gradient followed by pellet resuspension in PBS with 1 % BSA (BSA Fraction V, Sigma-Aldrich, Cat# 10735096001). Vessels were transferred onto a 40µm cell strainer (Corning, Cat# 431750) and extensively washed with cold PBS (with 250 ml). Isolated vessels were collected by washing the inverted cell strainer with PBS and centrifugation at 3000 *g* for 5 min.

Protein extraction

Isolated BECs and human iECs

Protein was extracted from isolated BECs and iECs with RIPA buffer containing 150 mM NaCl (Roth, Cat# 3957.1), 1 M Tris-HCl pH 7.5 (Roth, Cat# 9090.3), 1 % NP40 (Sigma Alrich Cat# 74385), 0.5 % Deoxycholate (Roth, Cat# 3484.3), and 0.1 % SDS (Serva, Cat# 20765.03) and protein inhibitors cocktail (Roche, Cat# 4693159001). Samples were incubated in RIPA buffer for 30min on ice followed by centrifugation at 18,000 *g* for another 30 min at 4 °C. Supernatants were collected and kept at -80 °C for further analysis.

Isolated vessels

Isolated vessels were lysed in a buffer containing 100 mM Tris-Hcl pH 7.6 (Roth, Cat# 9090.3), 4 % SDS (Serva, Cat# 20765.03) and 100 mM DTT (Sigma, Cat# 3483-12-3) by homogenization with a dounce tissue grinder (Wheaton) and heating for 3min at 95ºC. After lysis, samples were sonicated (30 sec, amplitude 100 %, duty cycle 50 %) 5 times with intermediate cooling using VialTweeter sonicator (Hielscher). Remaining undissolved material and cell debris were removed by centrifugation at 16,000 *g* for 15 min at 4 ºC. Supernatants were collected and kept at -80 ºC for further analysis.

Full brain tissue homogenization

Full tissue was homogenized in RIPA buffer containing 150 mM NaCl (Roth, Cat#3957.1), 1 M Tris-HCl pH 7.5 (Roth, Cat# 9090.3), 1 % NP40 (Sigma Alrich Cat#74385), 0.5 % Deoxycholate (Roth, Cat# 3484.3), 0.1 % SDS (Serva,

Cat#20765.03) and protein inhibitors cocktail (Roche, Cat# 4693159001) with a TissueLyzer and 5 mm steel beads (Qiagen). Samples were homogenized at 50 Hz for 3 min followed by 30 min incubation of ice. After RIPA incubation samples were centrifuged at 16,000 *g* for 30 min and supernatants were collected and kept at -80 ºC for further analysis.

Mass spectrometry and data analysis

Sample preparation

The whole sample of acutely isolated BECs (~5 µg) and 20 µg of full brain tissue lysates according to a BCA assay were subjected to proteolytical digestion using the single-pot solid-phase enhanced sample preparation (SP3)[104]. After 1:2 dilution with water, a benzonase digestion with 12.5 units was performed to remove remaining DNA/RNA. Proteins were reduced by addition of dithiothreitol (Biozol, Germany) in 50 mM ammonium bicarbonate to a final concentration of 10 mM and incubation for 30 min at 37°C. Cysteine residues were alkylated by addition of iodoacetamide (Sigma Aldrich, US) to a final concentration of 40 mM and incubation for 30 min at room temperature in the dark. Afterwards, the reaction was quenched by adding dithiothreitol.

Proteins were bound to 40 µg of a 1:1 mixture of hydrophilic and hydrophobic magnetic Sera-Mag SpeedBeads (GE Healthcare, US) using a final concentration of 70 % (v/v) acetonitrile for 30 min at room temperature. Beads were washed four times with 200 µL 80 % (v/v) ethanol. For proteolytic digestion, LysC (Promega, Germany) was added in 20 µL 50 mM ammonium bicarbonate with a protease to protein ratio of 1:80. Samples were incubated on a Thermomixer (Eppendorf, Germany) for 30 min at 1000 rpm and 37°C. Afterwards, trypsin (Promega, Germany) was added in 20 µL 50 mM ammonium bicarbonate with a protease to protein ratio of 1:80 followed by an incubation for 16 h at room temperature. Beads were retained with a magnetic rack and the supernatants were collected. Next, 20 µL 0.1% formic acid were added to the magnetic beads followed by sonication for 30 s in a sonication bath (Hielscher Ultrasonics GmbH, Germany). The supernatants of each sample were combined, filtered with 0.22 µm spin filters (Costar Spin-x, Corning, USA) to remove remaining beads, and dried by vacuum centrifugation. Dried peptides were

dissolved in 20 µL 0.1% formic. The peptide concentration after proteolytic digestion was estimated using the Qubit protein assay (Thermo Fisher Scientific, US).

Isolated brain vessels were processed in the same fashion with following alterations. Subsequent to the benzonase digest, samples were immediately bound to 20µg of the Sera-Beads mixture, alkylated and the reaction was quenched as described. After an additional bead binding step, using a final concentration of 70% (v/v) acetonitrile, samples were further processed according to the standard SP3 protocol.

Mass spectrometry

The isolated BEC, isolated vessel, and full tissue samples were analyzed on a nanoLC system (EASY-nLC 1200, Thermo Scientific, US) which was coupled online via a nanospray flex ion source (Proxeon – part of Thermo Scientific, US) equipped with a PRSO-V2 column oven (Sonation, Germany) to a Q-Exactive HF mass spectrometer (Thermo Scientific, US).

A peptide amount of 1 µg per sample was separated on a nanoLC system (EASY-nLC 1200, Thermo Scientific, US) using an in-house packed C18 column (30 cm x 75 µm ID, ReproSil-Pur 120 C18-AQ, 1.9 µm, Dr. Maisch GmbH, Germany) with a binary gradient of water (A) and acetonitrile (B) containing 0.1% formic acid at 50°C column temperature and a flow rate of 250 nl/min (gradient: 0 min, 2 % B; 3:30 min, 5 % B; 137:30 min, 25 % B; 168:30 min, 35 % B; 182:30 min, 60 % B). Full MS spectra were acquired at a resolution of 120,000. The top 15 peptide ions were chosen for Higher-energy C-trap Dissociation (HCD) with a normalized collision energy of 26 %. Fragment ion spectra were acquired at a resolution of 15,000. A dynamic exclusion of 120 s was used for peptide fragmentation.

The comparison of acutely isolated endothelial cells and brain homogenates, Arf6-Ko mouse BECs, as well as iPSC derived human endothelial cells were analyzed on a nanoElute nanoHPLC which was coupled to a TimsTOF pro mass spectrometer with a CaptiveSpray ion source (Bruker, Germany).

An amount of 350 ng of peptides were separated on a on an in-house packed C18 analytical column (15 cm × 75 µm ID, ReproSil-Pur 120 C18-AQ, 1.9 µm, Dr. Maisch GmbH) using a binary gradient of water and acetonitrile (B) containing 0.1% formic acid at flow rate of 250 nL/min (0 min, 2 % B; 2 min, 5% B; 70 min,

24 % B; 85 min, 35 % B; 90 min, 60 % B) and a column temperature of 50°C. For the comparison of BEC vs full tissue, a standard Data Dependent Acquisition Parallel Accumulation–Serial Fragmentation (DDA-PASEF) method with a cycle time of 1.1 s was used for spectrum acquisition. Briefly, ion accumulation and separation using Trapped Ion Mobility Spectrometry (TIMS) was set to a ramp time of 100 ms. One scan cycle included one TIMS full MS scan and 10 PASEF peptide fragmentation scans. The m/z scan range was set to 100-1700 for both, MS and MS/MS scans. The ion mobility scan range was set to 1/k0 0.75-1.40.
For Arf6-Ko mouse BECs and human iECs, a Data Independent Acquisition Parallel Accumulation–Serial Fragmentation (DIA-PASEF) method was used for spectrum acquisition. Ion accumulation and separation using Trapped Ion Mobility Spectrometry (TIMS) was set to a ramp time of 100 ms. One scan cycle included one TIMS full MS scan and with 26 windows with a width of 27 m/z covering a m/z range of 350-1002 m/z. Two windows were recorded per PASEF scan. This resulted in a cycle time of 1.4 s.

Data Analysis

The DDA raw data was analyzed by the software Maxquant (maxquant.org, Max-Planck Institute Munich) version 1.6.3.4, or 2.0.1.0[105,106]. The MS data was searched against a one protein per gene canonical fasta databases of Mus musculus (downloads: September 09th 2020, 21997 entries or February the 10th 2021, 21998 entries) from UniProt. Trypsin was defined as protease. Two missed cleavages were allowed for the database search. The option first search was used to recalibrate the peptide masses within a window of 20 ppm. For the main search peptide mass tolerances were set to 4.5 and 10 ppm for the Orbitrap and TOF mass spectrometer, respectively. Peptide fragment mass tolerances were set to 20 and 40 ppm for the Orbitrap and TOF mass spectrometer, respectively. Carbamidomethylation of cysteine was defined as static modification. Acetylation of the protein N-term as well as oxidation of methionine were set as variable modifications. The false discovery rate for both peptides and proteins were adjusted to less than 1 %. Label free quantification (LFQ) of proteins required at least two ratio counts of unique peptides. The option “match between runs” was enabled with a matching time of 1 min and an ion mobility window of 0.05 1/k0.

The DIA-PASEF raw data was analyzed with the software DIA-NN version 1.8 (https://github.com/vdemichev/DiaNN)[107] using a library-free search against a one protein per gene database from either Mus musculus or Homo sapiens according to the sample type (murine DB: download date: 2023-01-17, 21976 entries; human DB: 2023-03-01, 20603 entries). Trypsin was defined as protease and 2 missed cleavages were allowed. Oxidation of methionines and acetylation of protein N-termini were defined as variable modifications, whereas carbamidomethylation of cysteines was defined as fixed modification. The precursor and fragment ion m/z ranges were limited from 350 to 1001 and 200 to 1700, respectively. Precursor charge states of 2-4 were considered. The optimal mass accuracy for peptides and peptide fragments as well as the ion mobility tolerances were automatically determined by DIA-NN. An FDR threshold of 1% was applied for peptide and protein identifications.

The protein LFQ intensities were log2 transformed and two-sided Student's t-test was applied between the groups for statistical evaluation of differential protein abundance. If more than two groups were compared with each other, a one-way Anova test was additionally applied. To account for multiple hypotheses, a permutation-based FDR correction was applied separately for each comparison[108]. Only proteins with at least three valid values per group were considered for relative quantification.

Cluster analysis of protein expression changes

Time-series clustering was performed using an unsupervised, nonparametric model-based method, the Dirichlet process Gaussian process mixture model (DPGP, https://github.com/PrincetonUniversity/DP_GP_cluster)[39] on the zero transformed mean log2 LFQ values of all 2516 quantified proteins. In brief, two important considerations in this problem are (1) selecting the "correct" or "optimal" number of clusters and (2) modeling the trajectory and time-dependency of protein expression. A Dirichlet process can determine the number of clusters in a nonparametric manner, while a Gaussian process can model the trajectory and time-dependency of protein expression in a nonparametric manner. Optimal clustering was selected using the 'maximum a posteriori' (MAP) criterion.

Enrichment analysis

Gene Ontology enrichment analyses of subcellular localization (GOTERM_CC-DIRECT) and biological processes (GOTERM_BP_DIRECT) in BEC protein expression clusters were performed with DAVID (Database for Annotation, Visualization and Integrated Discovery, version 6.8) software using all identified BEC proteins as a background dataset[109]. We analyzed each expression clusters (1-16) separately focusing on significantly altered proteins during aging (Anova, p-value < 0,05). Among the annotation results we selected the significantly enriched GO terms (Fisher Exact test, FDR p-value < 0.05).

Enrichment analysis of human disorders in the aged BEC proteome (18 versus 3 month of age) was performed with WebGestalt (WEB-based GEne SeT AnaLysis Toolkit) software[110] using the Over-Representation Analysis (ORA) module with the Disease GLAD4U functional database and protein-coding genome reference dataset[111]. Among the annotation results we selected the top 25 disease terms showing association (Fisher Exact test, FDR p-value < 0,05) with our input dataset.

Protein network analysis and visualization

Protein-protein interaction networks were constructed and visualized with STRING (version 11.0) and Cytoscape (version 3.8.2) software, respectively. We selected experimentally determined protein interactions having minimum medium confidence (interaction score >0.4) in the *Mus musculus* database. The color gradients and size of nodes were set based on the fold change and p-value of protein changes at 18 compared to 3 months of age. Proteins were filtered based on the significance level of protein changes at 18 compared to 3 months of age (t-test, p < 0.05). Additional filter settings were applied in Cytoscape (version 3.8.2) based on the gene of interest (see Results).

iPSC Cell culture

iPSC experiments were performed in accordance with all relevant local guidelines and regulations. Work was done with the female iPSC line A18944 that is commercially available (ThermoFisher, Cat# A18945). iPSCs were maintained on vitronectin-coated (ThermoFisher Cat# A14700) culture plates and grown until reaching 80 % confluency in Essential 8 Flex Medium (ThermoFisher Cat#

A2858501) at 37 ºC with 5 % CO_2. Cells were routinely passaged using PBS-500nM EDTA (ThermoFisher, Cat# 15575020).

CRISPR/Cas9 Genome

A previously described single guide RNA (sgRNA) for targeting APOE exon2[112] was used for the genome editing. The sgRNA sequence (GGTTCTGTGGGCTGCGTTGC) was cloned into the MLM3636 plasmid (a gift from K. Joung, Adgene Cat# 43860) using the BsmBI restriction site. Genome editing was conducted as previously described[113] using Cas9 plasmid pSpCas9(BB)-2A-Puro (PX459) V2.0 (a gift from F. Zhang, Addgene Cat# 62988). For electroporation, cells were dissociated using Accutase (ThermoFisher, Cat# A1110501), transferred to Geltrex-coated (ThermoFisher Cat# A1413302) culture plates and grown in StemFlex (ThermoFisher Cat# A3349401) containing 10mM ROCK inhibitor (Selleckchem Cat# S1049) for two days at a density of 150k cells/cm^2. iPSCs were transfected by electroporation as previously described[114] with some modifications. Briefly, two million cells were resuspended in 100µL electroporation solution (VWR, Cat# MIR50117) containing 20 µg Cas9 and 5µg sgRNA plasmid. Cells were electroporated with 2 pulses at 65mV for 20ms in a 1mm cuvette (Fisher Scientific, Cat# 15437270) and plated onto Geltrex-coated 10-cm plates with StemFlex medium containing 10mM ROCK inhibitor. One day after electroporation, cells expressing Cas9 were selected with 350ng/mL Puromycin dihydrochloride (VWR, Cat# J593) for three consecutive days as shown previously[115]. Single-cell clone colonies were picked and analyzed by restriction fragment length polymorphism (RFLP) using NEB enzyme BbvI and Sanger sequencing as previously described[114].

To accommodate for improvements in the genome editing field, the previous protocol was modified for RNP-based DNA cleavage[116] of the ARF6 locus. A sgRNA targeting ARF6 exon2 (GGAAATGCGGATCCTCATGT) was ordered from Synthego. Similarly, for electroporation, iPSCs were seeded onto Geltrex-coated plates at a density of 150k cells/cm^2 for two days in StemFlex and ROCK inhibitor. To prepare the RNP complex, 60pmol of sgRNA was mixed with 30pmol of high-fidelity Cas9 mutant (IDT, Cat##1081060) and incubated for 15min at RT. For the electroporation, 200k cells were ressuspended in 20µL of P3 Primary Cell Nucleofector Solution (Lonza, Cat# V4XP-3032) and mixed gently with the RNP

complex. Cells were transferred onto one well of a nucleocuvette strip (Lonza, Cat# V4XP-3032) and electroporated in a 4DNucleofactor X Unit (Lonza, Cat# AAF-1002X) using the program CA137. After electroporation, cells were plated in one 12w Geltrex-coated culture plated with StemFlex and 1X RevitaCell (ThermoFisher, Cat# A2644501) for 2-4 days. Cells were then seeded at low density and single-cell clones colonies were picked and analyzed by RFLP using NEB enzyme Fat I followed by Sanger sequencing as described previously[114].

The knockouts were confirmed on protein level either using Western blot analysis of RIPA lysates or proteomics, respectively. For quality control, we checked for off-target effects by PCR amplification and Sanger sequencing of the top five most likely loci based on MIT and CFD scores from CRISPOR (http://crispor.tefor.net/,[117]). We also excluded on-target effects such as loss-of-heterozygosity using nearby SNP sequencing[118]. Lastly, pluripotency was confirmed through immunofluorescence staining of OCT4, NANOG, SSEA4, and TRA160, and chromosomal integrity was validated by molecular karyotyping (LIFE & BRAIN GmbH).

iPSC differentiation into human endothelial cells (iECs)

iPSCs were seeded onto Geltrex-coated (ThermoFisher Cat# A1413302) cell culture plates at a density of 200k cell/cm^2 in StemFlex medium (ThermoFisher Cat# A3349401) containing 10mM of ROCK inhibitor (Selleckchem Cat# S1049). Differentiation was started 24h after seeding by switching medium to Mesoderm Induction Media (StemCell, Cat# 05220). Medium was replenished every 24h for 2 days. On day 3, medium was switched to APEL2 medium (StemCell, Cat# 05270) supplemented with 200 ng/mL VEGF (Peprotech, Cat# 100-20) and 2µM Forskolin (Peprotech, Cat# 6652995). Medium was also replenished every 24h for 2 days. On day 5, endothelial cells were selected for CDH5 via magnetic sorting: cells were dissociated using accutase (ThermoFisher, Cat# A1110501) and incubated with CDH5 MicroBeads (Milteny Biotec, Cat# 130-097-867) following manufacturer's instructions. CD144+ fraction was plated onto Collagen IV-coated (Sigma Aldrich, Cat# C5533-5MG) culture plates at a density of 200k/cm^2 and grown in endothelial cell medium (PromoCell, Cat# C-22011). Endothelial cells were grown until reaching 80-95% confluency and passaged

with Trypsin-EDTA (ThermoFisher, Cat# 25200056) to a ratio of 1:2-1:6. Cells were cultured up to 5 passages.

FM1-43FX treatment in vitro

iECs were seeded onto ColIV-coated plates and grown until reach confluence. Cells were incubated for 15min at 37ºC with 5μg/mL of FM1-43FX (ThermoFisher, Cat#F35355) diluted in ddH20. After PBS washing, cells were fixed with 4% PFA for further analysis.

AAV-based overexpression of Arf6

pArf6-EGFP (#49649)[119] was obtained from Addgene. pAAV-CAG-GFP was a gift from Edward Boyden (Addgene plasmid #37825). pArf6-EGFP served as template to clone pArf6-2a-EGFP vectors via standard cloning techniques.

Arf6 overexpression in mouse BECs

For *in vivo* work, adeno-associated viral particles (AAV) were produced according to a previously described protocol[120]. Shortly, HEK293T (ATCC, #CRL-3216) cells were grown in DMEM (high glucose, GlutaMAX) supplemented with 10% fetal bovine serum (FBS) and 5% Pen Strep. Cells were transfected using polyethylenimine (PEI) solution with a 1:4:2 molar ratio of helper (pXX6)[121], capsid (pXX2-187-NRGTEWD)[55] and desired construct plasmids (pArf6-2a-EGFP or pAAV-CAG-GFP) in DPBS medium without glutamine and serum. 24 hours after transfection, media was changed back to serum supplemented DMEM and the cells were kept for 3 days before harvesting. Supernatant was harvested at 72h and 120h after transfection and kept at 4°C. 120 hours after cells were scraped, they were mixed with SAN + SAN digestion buffer and incubated at 37 °C in a water bath for 1 hour. The supernatant was then combined with PEG solution overnight and subsequently centrifuged at the speed of 4000 g for 30 minutes at 4 °C. The resulting PEG pellet and cell lysate were mixed together and loaded on top of an iodoxanol gradient and centrifuged at 350,000 g for 2 hours and 25 minutes at 18 °C with slow acceleration. Once the virus was collected from the iodoxanol gradient, it was passed through an Amicon filter and washed multiple times to remove iodoxanol. After the final wash, the virus was resuspended and collected from the filter. Titers were determined using qPCR.

Viral aliquots were stored at -80°C until used. AAVs (GFP or ARF6-GFP) were administered intravenously in 2 months old C57BL6J mice at a dose of 2×10^{10} viral particles/mouse. BEC were isolated 4 weeks post infection.

Arf6 overexpression in human iECs

For *in vitro* work, AAV particles were produced in HEK293T cells. Cells were grown in DMEM supplemented with 10% FBS and Penicillin- Streptomycin until reaching 80% confluency. Upon confluency, cells were triple transfected with pHelper, pAAV-DJ (CellBioLabs, Cat# VPK-400-DJ) and pAAV-GFP or pAAV-ARF6-GFP using polyethylenimine (PEI), pH 7.0.

Cells were detached using 0.5M EDTA in PBS, pH 7.4 two to three days after transfection. AAV particles were extracted using AAVpro Purification kit (All serotypes) (Takara, Cat# 6666) and titration was performed by qPCR using AAVpro Titration Kit (for Real Time PCR) Ver.2 (Takara, Cat# 6233) in both cases following manufacturer's instructions.

Cells were seeded onto ColIV-coated plates one day before the AAV treatment into a 50% confluency approximately. 24h after seeding cells were treated with 3 x 10^7 viral particles/well (GFP or ARF6-GFP) in ECM and incubated for another 48h, when media was exchanged to ECM. Cells were collected for MS analysis 4 days after viral infection.

Immunohistochemistry

Supplementary Table 9 specifies the primary and secondary antibodies used in the present study including working dilutions.

Brain slices

Brain samples were embedded in 3 % agarose for 100 µm coronal vibratome sectioning. Coronal free-floating sections were permeabilized and blocked using 3 % BSA / TritonX100 for 1h at room temperature (RT). Primary antibodies were diluted in 3 % BSA in PBS and incubated overnight at 4 ºC. Secondary antibodies were diluted in PBS and incubated at RT for 2h. After washing, DNA was stained using DAPI (Invitrogen Cat# D1306, 1:2000) for 5 min at RT. Brain slices were mounted using Fluoromount medium (Sigma-Aldrich, Cat# F4680-25ML).

Isolated BECs

Isolated BECs were fixed in suspension using 4 % PFA for 20 min at RT. After PFA washing via centrifugation at 2000 *g* for 10 min, cells were resuspended in dH_2O water, transferred onto a microscope slide (ThermoFisher Cat# J1800AMNZ) and dried at RT. Cells were blocked using 3 % BSA in PBS for 1h at RT. Primary antibodies were diluted in the same blocking buffer and incubated overnight at 4 ºC while secondary antibodies were diluted in PBS and incubated for 1 h at RT. After washing, DNA was stained using DAPI (Invitrogen Cat# D1306, 1:2000) for 5 min at RT. BECs were mounted using Fluoromount medium (Sigma-Aldrich, Cat# F4680-25ML).

Isolated vessels

Isolated vessels were transferred onto a microscope slide (ThermoFisher Cat# J1800AMNZ) and dried at RT. Fixation and permeabilization was performed using ice-cold 100 % acetone for 10 min at -20 ºC followed by blocking with 3% BSA in PBS for 1 h at RT. Primary antibodies were diluted in the same blocking buffer and incubated overnight at 4ºC while secondary antibodies were diluted in PBS and incubated 1 h at RT. After washing, DNA was stained using DAPI (Invitrogen Cat# D1306, 1:2000) for 5 min at RT. Isolated vessels were mounted mounted using Fluoromount medium (Sigma-Aldrich, Cat# F4680-25ML).

Differentiated human endothelial cells (iECs)

Differentiated endothelial cells were seeded into Collagen-IV (Sigma Aldrich, Cat# C5533-5MG) coated coverslips and fixed with 4 % PFA for 15 min at RT when reached a confluent monolayer. After washing, cells were blocked using 3% BSA buffer in PBS for 1h at RT. Primary antibodies were diluted in the same blocking buffer and incubated overnight at 4ºC. Secondary antibodies were diluted in PBS and incubated 1 h at RT. After washing, DNA was stained using DAPI Invitrogen Cat# D1306, 1:2000) for 5 min at RT. Coverslips with endothelial cells were mounted using Fluoromount medium (Sigma-Aldrich, Cat# F4680-25ML).

Confocal microscopy and image analysis

Fluorescent images were acquired with Zeiss Confocal microscope (LSM800, Zeiss, 40x objective with Airy-scan detector). Integrated density values of mo/hu Arf6 and Tfrc were determined using ImageJ software (version 1.52p) (10 images / sample), and normalized to Pecam1, Col4, or Cdh5 endothelial markers according to the experiments. Statistical significance was assessed by two-tailed Student's t test.

Transmission electron microscopy

Brain tissue

Mice were perfused in fixative (4 % PFA and 2.5 % glutaraldehyde in 0.1 M sodium cacodylate buffer, pH 7.4; Science Services) and brains immersion fixed for 24h, vibratome sectioned coronally and incubated for another 24h in the same fixative and stored in PBS. The sections were stored in PBS at 4°C until the start of the post-embedding. We applied a standard rOTO en bloc staining protocol (Kislinger et al., 2020) including post-fixation in 2% osmium tetroxide (EMS), 1.5% potassium ferricyanide (Sigma) in 0.1 M sodium cacodylate (Science Services) buffer (pH 7.4). Staining was enhanced by reaction with 1% thiocarbohydrazide (Sigma) for 45 min at 40 °C. The tissue was washed in water and incubated in 2% aqueous osmium tetroxide, washed and further contrasted by overnight incubation in 1 % aqueous uranyl acetate at 4 °C and 2 h at 50 °C. Samples were dehydrated in an ascending ethanol series and infiltrated with LX112 (LADD).

Isolated BECs

The isolated BEC pellet was conserved throughout all fixation, contrasting and infiltration steps. Cells were fixed for 15 min in 2.5 % glutaraldehyde (EM-grade, Science Services) in 0.1 M sodium cacodylate buffer (pH 7.4) (Sigma Aldrich), washed three times in 0.1 M sodium cacodylate buffer before postfixation in reduced osmium (1% osmium tetroxide (Science Services), 0.8 % potassium ferrocyanide (Sigma Aldrich) in 0.1 M sodium cacodylate buffer). After contrasting in 0.5 % uranylacetate in water (Science Services), the pellet was dehydrated in an ascending ethanol series, infiltrated in epon (Serva) and cured for 48 h at 60 °C.

Electron microscopy and image analysis

Ultrathin sections of brain tissues and BEC pellets were generated on a Leica UC7 and deposited onto formvar-coated copper grids (Science Services) without postcontrasting. Transmission Electron Microscopy images were acquired on a JEM 1400plus (JEOL) using the EMplified software (TVIPS, version 0.6.10).

Western blot and quantification

Protein lysates were analyzed by sodium dodecyl sulfate–polyacrylamide gel electrophoresis (SDS-PAGE) and transferred to 0.2 µm nitrocellulose membranes using the Mini-Protean and Trans-Blot system. After transfer, membranes were incubated in I-Block (Invitrogen, Cat# T2015) for 1 h at RT. Primary antibodies were incubated in the same buffer at 4 ºC overnight and horseradish peroxidase-conjugated secondary antibodies for 1h at RT. Detection was performed by chemiluminescence development (Immobilon ECL detection reagent, Merck Millipore) using Fusion FX7 (Vilber Lourmat). Protein levels were quantified using ImageJ Gel analyzer (version 1.52p). Statistical significance was analyzed by the two-tailed Student's t-test.The dilution of primary and secondary antibodies for Western blotting is specified in **Supplementary Table 9.**

Statistics and reproducibility

Data collection and analysis were not randomized. Blinding was applied to immunohistochemical image analysis. For all other experiments, blinding was not possible in order to preserve the homogeneity of the measurements (tissue processing and sample analysis were conducted alternately from the samples of the different experimental groups, avoiding batch effect and reducing technical variance). All data values of the descriptive statistics are given as mean ± s.d. unless stated otherwise. Data were analyzed using two-tailed unpaired t-test or ANOVA followed by Tukey's multiple comparisons test (indicated in each experiment, n=4-8 samples / group). For qualitative analysis experiments were repeated a minimum 4 times (**Fig. 1b, g**, **Fig. 5h, Extended data. Fig. 3b, Extended data. Fig. 5b**). No statistical methods were used to pre-determine sample sizes, but our sample sizes are similar to those reported in previous publications[102,103]. Data distribution was assumed to be normal but this was not formally tested. Beside the previously introduced software Excel (2016) and

GraphPad (8.3.1) were used for additional data analysis, statistics and figure representation. In case of APOE-KO vs WT human iEC proteomics experiment n=1 KO sample was excluded due to incomplete APOE deficiency.

Data Availability

The datasets generated through this work are available in a publicly accessible repository. The mass spectrometry proteomics data have been deposited to the ProteomeXchange Consortium via the PRIDE[122] partner repository with the dataset identifiers PXD045026, PXD045006, PXD045004, PXD044996, and PXD044993. All data supporting the findings described in this manuscript are available in the article and in the supplementary materials and from the corresponding author upon request. Source data are provided with this paper.

Acknowledgements

We thank Tom Webb for technical advice for the EC differentiation protocol, Yaw Asare and Ulrike Schillinger for help with the AAV injection, Barbara Lindner, Anna Berghofer, Lea Peischer, Melanie Schneider, and Alessia Nottebrock for the technical assistance. This study received funding from the European Union's Horizon 2020 research and innovation programme SVDs@target (No 666881, to MD) and European Innovation Council (EIC) programme (Grant Agreement #101115381, to MD); the Deutsche Forschungsgemeinschaft (DFG) as part of the Munich Cluster for Systems Neurology (SyNergy; EXC 2145 SyNergy – ID 390857198, to MD) and individual project grants (DI 722/13-1; DI 722/16-1, BE 6169/1-1, to MD), the Vascular Dementia Research Foundation, through the Federal Ministry for Education and Research (BMBF, CLINSPECT-M, to MD), a grant from the Leducq Foundation (grant agreement N022CVD01 to MD) ERA-NET Neuron (MatriSVDs, to MD), and the LMUexcellent fund (to MD). Graphics from Fig. 1a, 3a, 3b, 4a, 4e were created with Biorender.com.

Author contributions

K.T.V., J.G.G. and M.D. designed the project; S.A.M. and A.S. performed mass spectrometry; K.T.V., R.M., and N.B. analyzed proteomics experiments; K.T.V. and J.G.G. performed and analyzed biochemical and immunocytochemistry experiments; J.G.G., D.C., and S.R. performed gene editing and analyzed cell culture experiments; M.S. performed electron microscopy; M.I.T. designed and established the publicly available database; J.K. provided AAV-BR1 and F.B. produced Arf6-AAV for the *in vivo* experiments; M.D., S.L., D.P., M.S., C.H., and A.E. supervised the experiments, K.T.V., J.G.G. and M.D. wrote the manuscript; all authors read and revised the manuscript.

Competing interests

The authors declare no competing interests.

Figure legends

Figure 1. Proteomic analysis of mouse BECs during aging

a. Protocol for isolation of brain endothelial cells (BEC) for proteomics. **b**. Top: isolated capillaries (scale bar: 10 μm) and BECs (scale bar: 5 μm) stained for CD31, Cdh5, and Cldn5. Bottom: ultrastructure of isolated BECs from 3- and 18-months-old mice (scale bar: 1 μm) (1 – nucleus, 2 – cytoplasm, 3 – cytoplasmic protrusions, 4 – mitochondria, 5 – vacuoles, 6 - lysosomes, 7 – membrane inclusion). **c**. Left: Volcano plot shows enrichment of endothelial marker proteins (labelled with their gene name) in BEC preparations compared to full brain tissue (FT) (n=4 mice per group). Right: relative abundance of Nos3, Cdh5, and Pecam1 proteins in BECs (normalized to FT), and across different time points (normalized to 3 months). **d.** Summary of the LC–MS/MS and LFQ results. **e**. Correlation between age-related changes of the BEC proteome (current study) and transcriptome[45] focusing on overlapping significantly altered genes in both datasets. Red line marks simple linear regression ($p < 0.0001$). **f**. Left: Volcano plots show protein abundance changes during BEC aging (compared to 3-months of age, n=4-5 mice per group). Proteins showing the highest or most significant changes in abundance are marked with their gene names. Right: Relative abundance of neurofilament and myelin marker proteins in BECs (normalized to FT). **g**. Ultrastructural images of Mbp localization and multilamellar membranous structure engulfment (white arrowheads) by aged mouse brain endothelium in brain capillary (scale bar: 1 μm) and isolated BEC (scale bar: 1 μm (confocal) and 200 nm (EM)). **b** and **g**: experiments were repeated 6 times. **c** and **f**: -log10 transformed p-value plotted against the log2 transformed protein LFQ ratio for each protein. Comparison by two-tailed unpaired t-test. Dotted lines mark FDR threshold ($p < 0.05$). Red and blue color indicate significant ($p < 0.05$) enrichment and depletion, respectively. Bar graphs represent mean values +/- SEM, data points are from individual animals (***$p < 0.001$). The exact p-values are presented in source data file for Figure 1.

Figure 2. Unsupervised clustering of age-related protein dynamics of BECs

a. Enrichment analysis of subcellular localization and biological processes of significantly altered proteins by clusters based on Gene Ontology (GO) terms

(FDR $p < 0.05$). Clusters were determined by the Dirichlet process Gaussian process mixture model on the zero transformed mean log2 LFQ values. **b.** Exemplary clusters illustrating variations in the pattern of age-related protein abundance changes. (Blue line: cluster mean, light blue band: confidence interval, yellow line: all quantified, red line: significant protein abundance in each cluster). **c.** Heatmap of significantly altered proteins according to biological processes and selected clusters ordered by directionality of change (normalized on 3 months) (comparison by ANOVA followed by Tukey's multiple comparisons test, $p < 0.05$).

Figure 3. Age-related changes of BEC proteins implicated in vesicular transport

a. Endothelial vesicle-mediated transport pathways and associated proteins that were significantly up- (red) or downregulated (blue) in BECs during aging (ANOVA, p-value < 0.05, n=5 mice per group). **b.** Age-related proteomic analysis and the lack of correlation between vesicle-mediated transport proteins of BECs compared to whole brain vasculature. Red line marks simple linear regression. **c.** Comparison of age-related proteome changes of endothelial vesicle-mediated transport in BECs versus whole brain vasculature (BV). BECs: Comparison by ANOVA followed by Tukey's multiple comparisons test ($p < 0.05$). Vessels: Comparison by two-tailed unpaired t-test ($p < 0.05$). **d.** Detailed results of selected proteins (n=4-5 mice per group). **e.** Immunocytochemistry and quantification of Arf6 and Tfrc in isolated BECs (scale bar: 2 µm) and isolated brain vessels (scale bar: 20 µm) of young and aged mice (n=5-6 mice per group). White arrows and arrowheads indicate the cytoplasmic and membrane localization of Tfrc, respectively. **d, e**: Comparison by two-tailed unpaired t-test ($p < 0.05$). Graphs represent mean values +/- SEM, data points are from individual animals (*$p < 0.05$, **$p < 0.01$; ***$p < 0.001$; ns, not significant). The exact p-values are presented in source data file for Figure 3.

Figure 4. Effects of endothelial Arf6 on vesicular transport and mRNA processing

a. Gene deletion and overexpression experiments on Arf6 in mice. **b.** Volcano plot showing differences in mouse BEC protein abundance between endothelial

Arf6-deficient and WT mice (n=8 mice per group). **c.** Summary of the LC–MS/MS results and enrichment analysis of significant downregulated proteins. **d.** Heatmap of top 27 most significantly altered vesicle-mediated transport proteins in Arf6-KO mouse BECs. **e.** Gene deletion and overexpression experiments on Arf6 in human iECs. **f.** Volcano plot showing differences in protein abundance between ARF6-deficient and WT cells human iECs (n=6 samples per group). **g.** Summary of the LC–MS/MS results and enrichment analysis of significant downregulated proteins. **h.** Heatmap of the top 27 most significantly altered vesicle-mediated transport proteins in ARF6-KO human iECs. **i.** Confocal validation of endothelial recombinant protein expression in AAV-treated mouse brain (scale bar: 20 µm). **j.** Confocal imaging and quantification of FM1-43X endocytosis in iECs (scale bar: 20 µm, comparison by two-tailed unpaired t-test ***$p < 0.001$). **i-j:** Graphs represent mean values +/- SEM, data points are from individual images. **k.** Volcano plot showing differences in mouse BEC protein abundance between Arf6- and Gfp-AAV treated mice (n=4 samples per group). **l.** Summary of the LC–MS/MS and LFQ results and enrichment analysis of significantly upregulated proteins. **m.** Heatmap of significantly altered vesicle-mediated transport proteins. **n**. Volcano plot showing differences in protein abundance between ARF6- and GFP-AAV treated human iECs (n=6 samples per group). **o.** Summary of the LC–MS/MS results and enrichment analysis of significantly upregulated proteins. **p.** Heatmap of the top 27 most significantly altered vesicle-mediated transport proteins. **b, f, k, n.** The -log10 transformed p-value is plotted against the log2 transformed protein LFQ ratio for each protein. Vesicle-mediated transport proteins highlighted in darker color. **b, d, f, h, k, m, n, p.** Comparison by two-tailed unpaired t-test ($p < 0.05$). Red and blue color indicate significant enrichment and depletion, respectively. The exact p-values are presented in source data file for Figure 4.

Figure 5. Apoe-deficiency causes a proteomic signature of accelerated BEC aging

a. Overrepresentation analysis of human brain diseases (count: number of significantly altered proteins, ER: enrichment ratio, neurodegenerative disorders highlighted in grey). **b.** Individual protein changes related to Alzheimer's disease (AD), Parkinson's disease (PD) and vascular dementia (VaD) during BEC aging

(normalized to 3 months of age, comparison by ANOVA followed by Tukey's multiple comparisons test, $p < 0.05$). **c.** Volcano plot showing differences in mouse BEC proteome of 3-months-old Apoe-deficient and WT mice (n=8 mice per group). Dotted lines mark an FDR threshold ($p < 0.05$, n=5 mice per group). **d.** Correlation of log2 transformed protein LFQ ratios that were significantly dysregulated in BECs from Apoe-KO and 18-months-old WT compared to 3-months-old WT animals. Red line marks a simple linear regression ($p < 0.0001$). **e.** Detailed results of selected proteins in 3-months-old Apoe-KO compared to WT mice. **f.** Interaction network of Arf6 and Apoe proteins with associated proteins that were significantly dysregulated in BECs at 18- versus 3 months of age. Colored edges indicate the interaction of hub-proteins. **g.** CRISPR/Cas9-genome editing and differentiation of human iPSCs to iECs. **h.** Western blot validation of APOE-KO iPSCs (experiment was repeated 4 times). **i.** Volcano plot shows protein abundance changes between APOE-KO and WT iECs (n=5-6 samples per group). Vesicle-mediated transport proteins are highlighted with darker color. **j.** Summary of the LC–MS/MS results and enrichment analysis of significantly downregulated proteins. **k.** Heatmap of top 27 most significantly altered vesicle-mediated transport proteins. **l.** Confocal imaging and quantification of FM1-43X endocytosis (scale bar: 20 µm). **c**, **e**, **f, i, k, l**: Comparison by two-tailed unpaired t-test ($p < 0.05$). **b, c, f, i, k, l**: Red and blue: significantly up- and downregulated proteins, respectively. **e**, **l**: Graphs represent mean values +/- SEM, data points are from individual mice (**e**) or images (**l**) (*$p < 0.05$, **$p < 0.01$; ***$p < 0.001$; ns, not significant). The exact p-values are presented in source data file for Figure 5.

References

1 Sweeney, M. D., Zhao, Z., Montagne, A., Nelson, A. R. & Zlokovic, B. V. Blood-Brain Barrier: From Physiology to Disease and Back. *Physiol Rev* **99**, 21-78 (2019). https://doi.org:10.1152/physrev.00050.2017

2 Siegenthaler, J. A., Sohet, F. & Daneman, R. 'Sealing off the CNS': cellular and molecular regulation of blood-brain barriergenesis. *Curr Opin Neurobiol* **23**, 1057-1064 (2013). https://doi.org:10.1016/j.conb.2013.06.006

3 Iadecola, C. The Neurovascular Unit Coming of Age: A Journey through Neurovascular Coupling in Health and Disease. *Neuron* **96**, 17-42 (2017). https://doi.org:10.1016/j.neuron.2017.07.030

4 Dunn, K. M. & Nelson, M. T. Neurovascular signaling in the brain and the pathological consequences of hypertension. *American journal of physiology. Heart and circulatory physiology* **306**, H1-14 (2014). https://doi.org:10.1152/ajpheart.00364.2013

5 Mattson, M. P. & Arumugam, T. V. Hallmarks of Brain Aging: Adaptive and Pathological Modification by Metabolic States. *Cell Metab* **27**, 1176-1199 (2018). https://doi.org:10.1016/j.cmet.2018.05.011

6 Lucin, K. M. & Wyss-Coray, T. Immune activation in brain aging and neurodegeneration: too much or too little? *Neuron* **64**, 110-122 (2009). https://doi.org:10.1016/j.neuron.2009.08.039

7 Sweeney, M. D., Sagare, A. P. & Zlokovic, B. V. Blood-brain barrier breakdown in Alzheimer disease and other neurodegenerative disorders. *Nat Rev Neurol* **14**, 133-150 (2018). https://doi.org:10.1038/nrneurol.2017.188

8 Jia, G., Aroor, A. R., Jia, C. & Sowers, J. R. Endothelial cell senescence in aging-related vascular dysfunction. *Biochim Biophys Acta Mol Basis Dis* **1865**, 1802-1809 (2019). https://doi.org:10.1016/j.bbadis.2018.08.008

9 Ungvari, Z. *et al.* Endothelial dysfunction and angiogenesis impairment in the ageing vasculature. *Nat Rev Cardiol* **15**, 555-565 (2018). https://doi.org:10.1038/s41569-018-0030-z

10 Donato, A. J., Machin, D. R. & Lesniewski, L. A. Mechanisms of Dysfunction in the Aging Vasculature and Role in Age-Related Disease. *Circ Res* **123**, 825-848 (2018). https://doi.org:10.1161/CIRCRESAHA.118.312563

11 Graves, S. I. & Baker, D. J. Implicating endothelial cell senescence to dysfunction in the ageing and diseased brain. *Basic Clin Pharmacol Toxicol* **127**, 102-110 (2020). https://doi.org:10.1111/bcpt.13403

12 Costea, L. *et al.* The Blood-Brain Barrier and Its Intercellular Junctions in Age-Related Brain Disorders. *Int J Mol Sci* **20** (2019). https://doi.org:10.3390/ijms20215472

13 Goodall, E. F. *et al.* Age-associated changes in the blood-brain barrier: comparative studies in human and mouse. *Neuropathol Appl Neurobiol* **44**, 328-340 (2018). https://doi.org:10.1111/nan.12408

14 Banks, W. A., Reed, M. J., Logsdon, A. F., Rhea, E. M. & Erickson, M. A. Healthy aging and the blood-brain barrier. *Nat Aging* **1**, 243-254 (2021). https://doi.org:10.1038/s43587-021-00043-5

15 Tarantini, S., Tran, C. H. T., Gordon, G. R., Ungvari, Z. & Csiszar, A. Impaired neurovascular coupling in aging and Alzheimer's disease: Contribution of astrocyte dysfunction and endothelial impairment to cognitive decline. *Exp Gerontol* **94**, 52-58 (2017). https://doi.org:10.1016/j.exger.2016.11.004

16 Tarumi, T. & Zhang, R. Cerebral blood flow in normal aging adults: cardiovascular determinants, clinical implications, and aerobic fitness. *J Neurochem* **144**, 595-608 (2018). https://doi.org:10.1111/jnc.14234
17 Brandes, R. P., Fleming, I. & Busse, R. Endothelial aging. *Cardiovascular research* **66**, 286-294 (2005). https://doi.org:10.1016/j.cardiores.2004.12.027
18 Donato, A. J., Morgan, R. G., Walker, A. E. & Lesniewski, L. A. Cellular and molecular biology of aging endothelial cells. *J Mol Cell Cardiol* **89**, 122-135 (2015). https://doi.org:10.1016/j.yjmcc.2015.01.021
19 Di Micco, R., Krizhanovsky, V., Baker, D. & d'Adda di Fagagna, F. Cellular senescence in ageing: from mechanisms to therapeutic opportunities. *Nat Rev Mol Cell Biol* **22**, 75-95 (2021). https://doi.org:10.1038/s41580-020-00314-w
20 Slack, R. J., Macdonald, S. J. F., Roper, J. A., Jenkins, R. G. & Hatley, R. J. D. Emerging therapeutic opportunities for integrin inhibitors. *Nat Rev Drug Discov* (2021). https://doi.org:10.1038/s41573-021-00284-4
21 Shin, E. Y. *et al.* Integrin-mediated adhesions in regulation of cellular senescence. *Sci Adv* **6**, eaay3909 (2020). https://doi.org:10.1126/sciadv.aay3909
22 Hafezi-Moghadam, A., Thomas, K. L. & Wagner, D. D. ApoE deficiency leads to a progressive age-dependent blood-brain barrier leakage. *Am J Physiol Cell Physiol* **292**, C1256-1262 (2007). https://doi.org:10.1152/ajpcell.00563.2005
23 Bell, R. D. *et al.* Apolipoprotein E controls cerebrovascular integrity via cyclophilin A. *Nature* **485**, 512-516 (2012). https://doi.org:10.1038/nature11087
24 Migrino, R. Q. *et al.* Amyloidogenic medin induces endothelial dysfunction and vascular inflammation through the receptor for advanced glycation endproducts. *Cardiovasc Res* **113**, 1389-1402 (2017). https://doi.org:10.1093/cvr/cvx135
25 Degenhardt, K. *et al.* Medin aggregation causes cerebrovascular dysfunction in aging wild-type mice. *Proceedings of the National Academy of Sciences of the United States of America* **117**, 23925-23931 (2020). https://doi.org:10.1073/pnas.2011133117
26 Migrino, R. Q. *et al.* Cerebrovascular medin is associated with Alzheimer's disease and vascular dementia. *Alzheimers Dement (Amst)* **12**, e12072 (2020). https://doi.org:10.1002/dad2.12072
27 Tabula Muris, C. A single-cell transcriptomic atlas characterizes ageing tissues in the mouse. *Nature* **583**, 590-595 (2020). https://doi.org:10.1038/s41586-020-2496-1
28 Ximerakis, M. *et al.* Single-cell transcriptomic profiling of the aging mouse brain. *Nat Neurosci* **22**, 1696-1708 (2019). https://doi.org:10.1038/s41593-019-0491-3
29 Angelidis, I. *et al.* An atlas of the aging lung mapped by single cell transcriptomics and deep tissue proteomics. *Nat Commun* **10**, 963 (2019). https://doi.org:10.1038/s41467-019-08831-9
30 Yang, A. C. *et al.* Physiological blood-brain transport is impaired with age by a shift in transcytosis. *Nature* **583**, 425-430 (2020). https://doi.org:10.1038/s41586-020-2453-z
31 Chen, M. B. *et al.* Brain Endothelial Cells Are Exquisite Sensors of Age-Related Circulatory Cues. *Cell Rep* **30**, 4418-4432 e4414 (2020). https://doi.org:10.1016/j.celrep.2020.03.012
32 Zhao, L. *et al.* Pharmacologically reversible zonation-dependent endothelial cell transcriptomic changes with neurodegenerative disease associations in the aged brain. *Nat Commun* **11**, 4413 (2020). https://doi.org:10.1038/s41467-020-18249-3

33 Aldridge, S. & Teichmann, S. A. Single cell transcriptomics comes of age. *Nat Commun* **11**, 4307 (2020). https://doi.org:10.1038/s41467-020-18158-5

34 Carlyle, B. C. *et al.* A multiregional proteomic survey of the postnatal human brain. *Nat Neurosci* **20**, 1787-1795 (2017). https://doi.org:10.1038/s41593-017-0011-2

35 Maier, T., Guell, M. & Serrano, L. Correlation of mRNA and protein in complex biological samples. *FEBS Lett* **583**, 3966-3973 (2009). https://doi.org:10.1016/j.febslet.2009.10.036

36 de Sousa Abreu, R., Penalva, L. O., Marcotte, E. M. & Vogel, C. Global signatures of protein and mRNA expression levels. *Mol Biosyst* **5**, 1512-1526 (2009). https://doi.org:10.1039/b908315d

37 Vogel, C. & Marcotte, E. M. Insights into the regulation of protein abundance from proteomic and transcriptomic analyses. *Nat Rev Genet* **13**, 227-232 (2012). https://doi.org:10.1038/nrg3185

38 Wang, D. *et al.* A deep proteome and transcriptome abundance atlas of 29 healthy human tissues. *Mol Syst Biol* **15**, e8503 (2019). https://doi.org:10.15252/msb.20188503

39 McDowell, I. C. *et al.* Clustering gene expression time series data using an infinite Gaussian process mixture model. *PLoS Comput Biol* **14**, e1005896 (2018). https://doi.org:10.1371/journal.pcbi.1005896

40 Rayon, T. *et al.* Species-specific pace of development is associated with differences in protein stability. *Science* **369** (2020). https://doi.org:10.1126/science.aba7667

41 Kim, D. S. *et al.* The dynamic, combinatorial cis-regulatory lexicon of epidermal differentiation. *Nat Genet* **53**, 1564-1576 (2021). https://doi.org:10.1038/s41588-021-00947-3

42 Shcherbina, A. *et al.* Dissecting Murine Muscle Stem Cell Aging through Regeneration Using Integrative Genomic Analysis. *Cell Rep* **32**, 107964 (2020). https://doi.org:10.1016/j.celrep.2020.107964

43 Garcia-Cabezas, M. A., John, Y. J., Barbas, H. & Zikopoulos, B. Distinction of Neurons, Glia and Endothelial Cells in the Cerebral Cortex: An Algorithm Based on Cytological Features. *Front Neuroanat* **10**, 107 (2016). https://doi.org:10.3389/fnana.2016.00107

44 Bjørnholm, K. D. *et al.* A robust and efficient microvascular isolation method for multimodal characterization of the mouse brain vasculature. *Cell Rep Methods* **3**, 100431 (2023). https://doi.org:10.1016/j.crmeth.2023.100431

45 Yousef, H. *et al.* Aged blood impairs hippocampal neural precursor activity and activates microglia via brain endothelial cell VCAM1. *Nat Med* **25**, 988-1000 (2019). https://doi.org:10.1038/s41591-019-0440-4

46 Schaum, N. *et al.* Ageing hallmarks exhibit organ-specific temporal signatures. *Nature* **583**, 596-602 (2020). https://doi.org:10.1038/s41586-020-2499-y

47 Zhou, T. *et al.* Microvascular endothelial cells engulf myelin debris and promote macrophage recruitment and fibrosis after neural injury. *Nat Neurosci* **22**, 421-435 (2019). https://doi.org:10.1038/s41593-018-0324-9

48 Safaiyan, S. *et al.* Age-related myelin degradation burdens the clearance function of microglia during aging. *Nat Neurosci* **19**, 995-998 (2016). https://doi.org:10.1038/nn.4325

49 Khalil, M. *et al.* Serum neurofilament light levels in normal aging and their association with morphologic brain changes. *Nat Commun* **11**, 812 (2020). https://doi.org:10.1038/s41467-020-14612-6

50 Eisen, M. B., Spellman, P. T., Brown, P. O. & Botstein, D. Cluster analysis and display of genome-wide expression patterns. *Proc Natl Acad Sci U S A* **95**, 14863-14868 (1998). https://doi.org:10.1073/pnas.95.25.14863

51 Chen, Z. *et al.* Reciprocal regulation of eNOS and caveolin-1 functions in endothelial cells. *Mol Biol Cell* **29**, 1190-1202 (2018). https://doi.org:10.1091/mbc.E17-01-0049

52 D'Souza-Schorey, C. & Chavrier, P. ARF proteins: roles in membrane traffic and beyond. *Nat Rev Mol Cell Biol* **7**, 347-358 (2006). https://doi.org:10.1038/nrm1910

53 Donaldson, J. G. Multiple roles for Arf6: sorting, structuring, and signaling at the plasma membrane. *J Biol Chem* **278**, 41573-41576 (2003). https://doi.org:10.1074/jbc.R300026200

54 Schweitzer, J. K. & D'Souza-Schorey, C. A requirement for ARF6 during the completion of cytokinesis. *Exp Cell Res* **311**, 74-83 (2005). https://doi.org:10.1016/j.yexcr.2005.07.033

55 Korbelin, J. *et al.* A brain microvasculature endothelial cell-specific viral vector with the potential to treat neurovascular and neurological diseases. *EMBO Mol Med* **8**, 609-625 (2016). https://doi.org:10.15252/emmm.201506078

56 Govindpani, K. *et al.* Vascular Dysfunction in Alzheimer's Disease: A Prelude to the Pathological Process or a Consequence of It? *J Clin Med* **8** (2019). https://doi.org:10.3390/jcm8050651

57 Malek, N. *et al.* Vascular disease and vascular risk factors in relation to motor features and cognition in early Parkinson's disease. *Mov Disord* **31**, 1518-1526 (2016). https://doi.org:10.1002/mds.26698

58 Iadecola, C. The pathobiology of vascular dementia. *Neuron* **80**, 844-866 (2013). https://doi.org:10.1016/j.neuron.2013.10.008

59 Cohen, R. M., Small, C., Lalonde, F., Friz, J. & Sunderland, T. Effect of apolipoprotein E genotype on hippocampal volume loss in aging healthy women. *Neurology* **57**, 2223-2228 (2001). https://doi.org:10.1212/wnl.57.12.2223

60 Espeseth, T. *et al.* Accelerated age-related cortical thinning in healthy carriers of apolipoprotein E epsilon 4. *Neurobiol Aging* **29**, 329-340 (2008). https://doi.org:10.1016/j.neurobiolaging.2006.10.030

61 Love, S. *et al.* Premorbid effects of APOE on synaptic proteins in human temporal neocortex. *Neurobiol Aging* **27**, 797-803 (2006). https://doi.org:10.1016/j.neurobiolaging.2005.04.008

62 den Heijer, T. *et al.* Hippocampal, amygdalar, and global brain atrophy in different apolipoprotein E genotypes. *Neurology* **59**, 746-748 (2002). https://doi.org:10.1212/wnl.59.5.746

63 Laursen, J. B. *et al.* Endothelial regulation of vasomotion in apoE-deficient mice: implications for interactions between peroxynitrite and tetrahydrobiopterin. *Circulation* **103**, 1282-1288 (2001). https://doi.org:10.1161/01.cir.103.9.1282

64 d'Uscio, L. V. *et al.* Mechanism of endothelial dysfunction in apolipoprotein E-deficient mice. *Arterioscler Thromb Vasc Biol* **21**, 1017-1022 (2001). https://doi.org:10.1161/01.atv.21.6.1017

65 Ohashi, M., Runge, M. S., Faraci, F. M. & Heistad, D. D. MnSOD deficiency increases endothelial dysfunction in ApoE-deficient mice. *Arterioscler Thromb Vasc Biol* **26**, 2331-2336 (2006). https://doi.org:10.1161/01.ATV.0000238347.77590.c9

66 Van Acker, T., Tavernier, J. & Peelman, F. The Small GTPase Arf6: An Overview of Its Mechanisms of Action and of Its Role in Host(-)Pathogen Interactions and Innate Immunity. *Int J Mol Sci* **20** (2019). https://doi.org:10.3390/ijms20092209

67 Palacios, F., Price, L., Schweitzer, J., Collard, J. G. & D'Souza-Schorey, C. An essential role for ARF6-regulated membrane traffic in adherens junction turnover and epithelial cell migration. *EMBO J* **20**, 4973-4986 (2001). https://doi.org:10.1093/emboj/20.17.4973

68 D'Souza-Schorey, C., Li, G., Colombo, M. I. & Stahl, P. D. A regulatory role for ARF6 in receptor-mediated endocytosis. *Science* **267**, 1175-1178 (1995). https://doi.org:10.1126/science.7855600

69 Song, L. & Pachter, J. S. Monocyte chemoattractant protein-1 alters expression of tight junction-associated proteins in brain microvascular endothelial cells. *Microvasc Res* **67**, 78-89 (2004). https://doi.org:10.1016/j.mvr.2003.07.001

70 Crewe, C. *et al.* An Endothelial-to-Adipocyte Extracellular Vesicle Axis Governed by Metabolic State. *Cell* **175**, 695-708 e613 (2018). https://doi.org:10.1016/j.cell.2018.09.005

71 Mathiesen, A. *et al.* Endothelial Extracellular Vesicles: From Keepers of Health to Messengers of Disease. *Int J Mol Sci* **22** (2021). https://doi.org:10.3390/ijms22094640

72 Blackburn, J. B., D'Souza, Z. & Lupashin, V. V. Maintaining order: COG complex controls Golgi trafficking, processing, and sorting. *FEBS Lett* **593**, 2466-2487 (2019). https://doi.org:10.1002/1873-3468.13570

73 Wagner, J. *et al.* Overexpression of the novel senescence marker beta-galactosidase (GLB1) in prostate cancer predicts reduced PSA recurrence. *PLoS One* **10**, e0124366 (2015). https://doi.org:10.1371/journal.pone.0124366

74 Debacq-Chainiaux, F., Erusalimsky, J. D., Campisi, J. & Toussaint, O. Protocols to detect senescence-associated beta-galactosidase (SA-betagal) activity, a biomarker of senescent cells in culture and in vivo. *Nat Protoc* **4**, 1798-1806 (2009). https://doi.org:10.1038/nprot.2009.191

75 Hipp, M. S., Kasturi, P. & Hartl, F. U. The proteostasis network and its decline in ageing. *Nat Rev Mol Cell Biol* **20**, 421-435 (2019). https://doi.org:10.1038/s41580-019-0101-y

76 Wan, B. *et al.* GIT1 protects traumatically injured spinal cord by prompting microvascular endothelial cells to clear myelin debris. *Aging (Albany NY)* **13**, 7067-7083 (2021). https://doi.org:10.18632/aging.202560

77 Johnsen, K. B., Burkhart, A., Thomsen, L. B., Andresen, T. L. & Moos, T. Targeting the transferrin receptor for brain drug delivery. *Prog Neurobiol* **181**, 101665 (2019). https://doi.org:10.1016/j.pneurobio.2019.101665

78 Terstappen, G. C., Meyer, A. H., Bell, R. D. & Zhang, W. Strategies for delivering therapeutics across the blood-brain barrier. *Nature reviews. Drug discovery* **20**, 362-383 (2021). https://doi.org:10.1038/s41573-021-00139-y

79 Okuyama, T. *et al.* Iduronate-2-Sulfatase with Anti-human Transferrin Receptor Antibody for Neuropathic Mucopolysaccharidosis II: A Phase 1/2 Trial. *Mol Ther* **27**, 456-464 (2019). https://doi.org:10.1016/j.ymthe.2018.12.005

80 Kariolis, M. S. *et al.* Brain delivery of therapeutic proteins using an Fc fragment blood-brain barrier transport vehicle in mice and monkeys. *Sci Transl Med* **12** (2020). https://doi.org:10.1126/scitranslmed.aay1359

81 Humphries, J. D., Byron, A. & Humphries, M. J. Integrin ligands at a glance. *J Cell Sci* **119**, 3901-3903 (2006). https://doi.org:10.1242/jcs.03098

82 Smith, J. W., Ruggeri, Z. M., Kunicki, T. J. & Cheresh, D. A. Interaction of integrins alpha v beta 3 and glycoprotein IIb-IIIa with fibrinogen. Differential peptide recognition accounts for distinct binding sites. *J Biol Chem* **265**, 12267-12271 (1990).
83 Silvestre, J. S. *et al.* Lactadherin promotes VEGF-dependent neovascularization. *Nat Med* **11**, 499-506 (2005). https://doi.org:10.1038/nm1233
84 Marazuela, P. *et al.* MFG-E8 (LACTADHERIN): a novel marker associated with cerebral amyloid angiopathy. *Acta Neuropathol Commun* **9**, 154 (2021). https://doi.org:10.1186/s40478-021-01257-9
85 Vanlandewijck, M. *et al.* Author Correction: A molecular atlas of cell types and zonation in the brain vasculature. *Nature* **560**, E3 (2018). https://doi.org:10.1038/s41586-018-0232-x
86 Hanayama, R. *et al.* Identification of a factor that links apoptotic cells to phagocytes. *Nature* **417**, 182-187 (2002). https://doi.org:10.1038/417182a
87 Tai, L. M. *et al.* The role of APOE in cerebrovascular dysfunction. *Acta Neuropathol* **131**, 709-723 (2016). https://doi.org:10.1007/s00401-016-1547-z
88 Yang, A. C. *et al.* A human brain vascular atlas reveals diverse cell mediators of Alzheimer's disease risk. *bioRxiv*, 2021.2004.2026.441262 (2021). https://doi.org:10.1101/2021.04.26.441262
89 Halliday, M. R. *et al.* Accelerated pericyte degeneration and blood-brain barrier breakdown in apolipoprotein E4 carriers with Alzheimer's disease. *Journal of cerebral blood flow and metabolism : official journal of the International Society of Cerebral Blood Flow and Metabolism* **36**, 216-227 (2016). https://doi.org:10.1038/jcbfm.2015.44
90 Carvalho, C. & Moreira, P. I. Oxidative Stress: A Major Player in Cerebrovascular Alterations Associated to Neurodegenerative Events. *Front Physiol* **9**, 806 (2018). https://doi.org:10.3389/fphys.2018.00806
91 Finkel, T. & Holbrook, N. J. Oxidants, oxidative stress and the biology of ageing. *Nature* **408**, 239-247 (2000). https://doi.org:10.1038/35041687
92 Johnson, A. A. & Stolzing, A. The role of lipid metabolism in aging, lifespan regulation, and age-related disease. *Aging Cell* **18**, e13048 (2019). https://doi.org:10.1111/acel.13048
93 Bazzoni, G. & Dejana, E. Endothelial cell-to-cell junctions: molecular organization and role in vascular homeostasis. *Physiol Rev* **84**, 869-901 (2004). https://doi.org:10.1152/physrev.00035.2003
94 Xiao, K. *et al.* p120-Catenin regulates clathrin-dependent endocytosis of VE-cadherin. *Mol Biol Cell* **16**, 5141-5151 (2005). https://doi.org:10.1091/mbc.e05-05-0440
95 Iyer, S., Ferreri, D. M., DeCocco, N. C., Minnear, F. L. & Vincent, P. A. VE-cadherin-p120 interaction is required for maintenance of endothelial barrier function. *Am J Physiol Lung Cell Mol Physiol* **286**, L1143-1153 (2004). https://doi.org:10.1152/ajplung.00305.2003
96 Armulik, A. *et al.* Pericytes regulate the blood-brain barrier. *Nature* **468**, 557-561 (2010). https://doi.org:10.1038/nature09522
97 Daneman, R. *et al.* The mouse blood-brain barrier transcriptome: a new resource for understanding the development and function of brain endothelial cells. *PLoS One* **5**, e13741 (2010). https://doi.org:10.1371/journal.pone.0013741
98 Diz, A. P., Truebano, M. & Skibinski, D. O. F. The consequences of sample pooling in proteomics: an empirical study. *Electrophoresis* **30**, 2967-2975 (2009). https://doi.org:10.1002/elps.200900210

99 Jang, S., Collin de l'Hortet, A. & Soto-Gutierrez, A. Induced Pluripotent Stem Cell-Derived Endothelial Cells: Overview, Current Advances, Applications, and Future Directions. *Am J Pathol* **189**, 502-512 (2019). https://doi.org:10.1016/j.ajpath.2018.12.004

100 Marquer, C. *et al.* Arf6 controls retromer traffic and intracellular cholesterol distribution via a phosphoinositide-based mechanism. *Nat Commun* **7**, 11919 (2016). https://doi.org:10.1038/ncomms11919

101 Sorensen, I., Adams, R. H. & Gossler, A. DLL1-mediated Notch activation regulates endothelial identity in mouse fetal arteries. *Blood* **113**, 5680-5688 (2009). https://doi.org:10.1182/blood-2008-08-174508

102 Monet-Lepretre, M. *et al.* Abnormal recruitment of extracellular matrix proteins by excess Notch3 ECD: a new pathomechanism in CADASIL. *Brain : a journal of neurology* **136**, 1830-1845 (2013). https://doi.org:10.1093/brain/awt092

103 Zellner, A. *et al.* CADASIL brain vessels show a HTRA1 loss-of-function profile. *Acta Neuropathol* **136**, 111-125 (2018). https://doi.org:10.1007/s00401-018-1853-8

104 Hughes, C. S. *et al.* Single-pot, solid-phase-enhanced sample preparation for proteomics experiments. *Nat Protoc* **14**, 68-85 (2019). https://doi.org:10.1038/s41596-018-0082-x

105 Cox, J. *et al.* Accurate proteome-wide label-free quantification by delayed normalization and maximal peptide ratio extraction, termed MaxLFQ. *Molecular & cellular proteomics : MCP* **13**, 2513-2526 (2014). https://doi.org:10.1074/mcp.M113.031591

106 Sinitcyn, P. *et al.* MaxDIA enables library-based and library-free data-independent acquisition proteomics. *Nat Biotechnol* (2021). https://doi.org:10.1038/s41587-021-00968-7

107 Demichev, V., Messner, C. B., Vernardis, S. I., Lilley, K. S. & Ralser, M. DIA-NN: neural networks and interference correction enable deep proteome coverage in high throughput. *Nat Methods* **17**, 41-44 (2020). https://doi.org:10.1038/s41592-019-0638-x

108 Tusher, V. G., Tibshirani, R. & Chu, G. Significance analysis of microarrays applied to the ionizing radiation response. *Proc Natl Acad Sci U S A* **98**, 5116-5121 (2001). https://doi.org:10.1073/pnas.091062498

109 Jiao, X. *et al.* DAVID-WS: a stateful web service to facilitate gene/protein list analysis. *Bioinformatics* **28**, 1805-1806 (2012). https://doi.org:10.1093/bioinformatics/bts251

110 Liao, Y., Wang, J., Jaehnig, E. J., Shi, Z. & Zhang, B. WebGestalt 2019: gene set analysis toolkit with revamped UIs and APIs. *Nucleic Acids Res* **47**, W199-W205 (2019). https://doi.org:10.1093/nar/gkz401

111 Jourquin, J., Duncan, D., Shi, Z. & Zhang, B. GLAD4U: deriving and prioritizing gene lists from PubMed literature. *BMC Genomics* **13 Suppl 8**, S20 (2012). https://doi.org:10.1186/1471-2164-13-S8-S20

112 Schmid, B. *et al.* Generation of a set of isogenic, gene-edited iPSC lines homozygous for all main APOE variants and an APOE knock-out line. *Stem Cell Res* **34**, 101349 (2019). https://doi.org:10.1016/j.scr.2018.11.010

113 Paquet, D. *et al.* Efficient introduction of specific homozygous and heterozygous mutations using CRISPR/Cas9. *Nature* **533**, 125-129 (2016). https://doi.org:10.1038/nature17664

114 Kwart, D., Paquet, D., Teo, S. & Tessier-Lavigne, M. Precise and efficient scarless genome editing in stem cells using CORRECT. *Nat Protoc* **12**, 329-354 (2017). https://doi.org:10.1038/nprot.2016.171
115 Steyer, B., Cory, E. & Saha, K. Developing precision medicine using scarless genome editing of human pluripotent stem cells. *Drug Discov Today Technol* **28**, 3-12 (2018). https://doi.org:10.1016/j.ddtec.2018.02.001
116 Skarnes, W. C., Pellegrino, E. & McDonough, J. A. Improving homology-directed repair efficiency in human stem cells. *Methods* **164-165**, 18-28 (2019). https://doi.org:10.1016/j.ymeth.2019.06.016
117 Concordet, J. P. & Haeussler, M. CRISPOR: intuitive guide selection for CRISPR/Cas9 genome editing experiments and screens. *Nucleic Acids Res* **46**, W242-W245 (2018). https://doi.org:10.1093/nar/gky354
118 Weisheit, I. *et al.* Simple and reliable detection of CRISPR-induced on-target effects by qgPCR and SNP genotyping. *Nat Protoc* **16**, 1714-1739 (2021). https://doi.org:10.1038/s41596-020-00481-2
119 Moorhead, A. M., Jung, J. Y., Smirnov, A., Kaufer, S. & Scidmore, M. A. Multiple host proteins that function in phosphatidylinositol-4-phosphate metabolism are recruited to the chlamydial inclusion. *Infect Immun* **78**, 1990-2007 (2010). https://doi.org:10.1128/IAI.01340-09
120 Challis, R. C. *et al.* Systemic AAV vectors for widespread and targeted gene delivery in rodents. *Nat Protoc* **14**, 379-414 (2019). https://doi.org:10.1038/s41596-018-0097-3
121 Xiao, X., Li, J. & Samulski, R. J. Production of high-titer recombinant adeno-associated virus vectors in the absence of helper adenovirus. *J Virol* **72**, 2224-2232 (1998). https://doi.org:10.1128/JVI.72.3.2224-2232.1998
122 Perez-Riverol, Y. *et al.* The PRIDE database resources in 2022: a hub for mass spectrometry-based proteomics evidences. *Nucleic Acids Res* **50**, D543-D552 (2022). https://doi.org:10.1093/nar/gkab1038

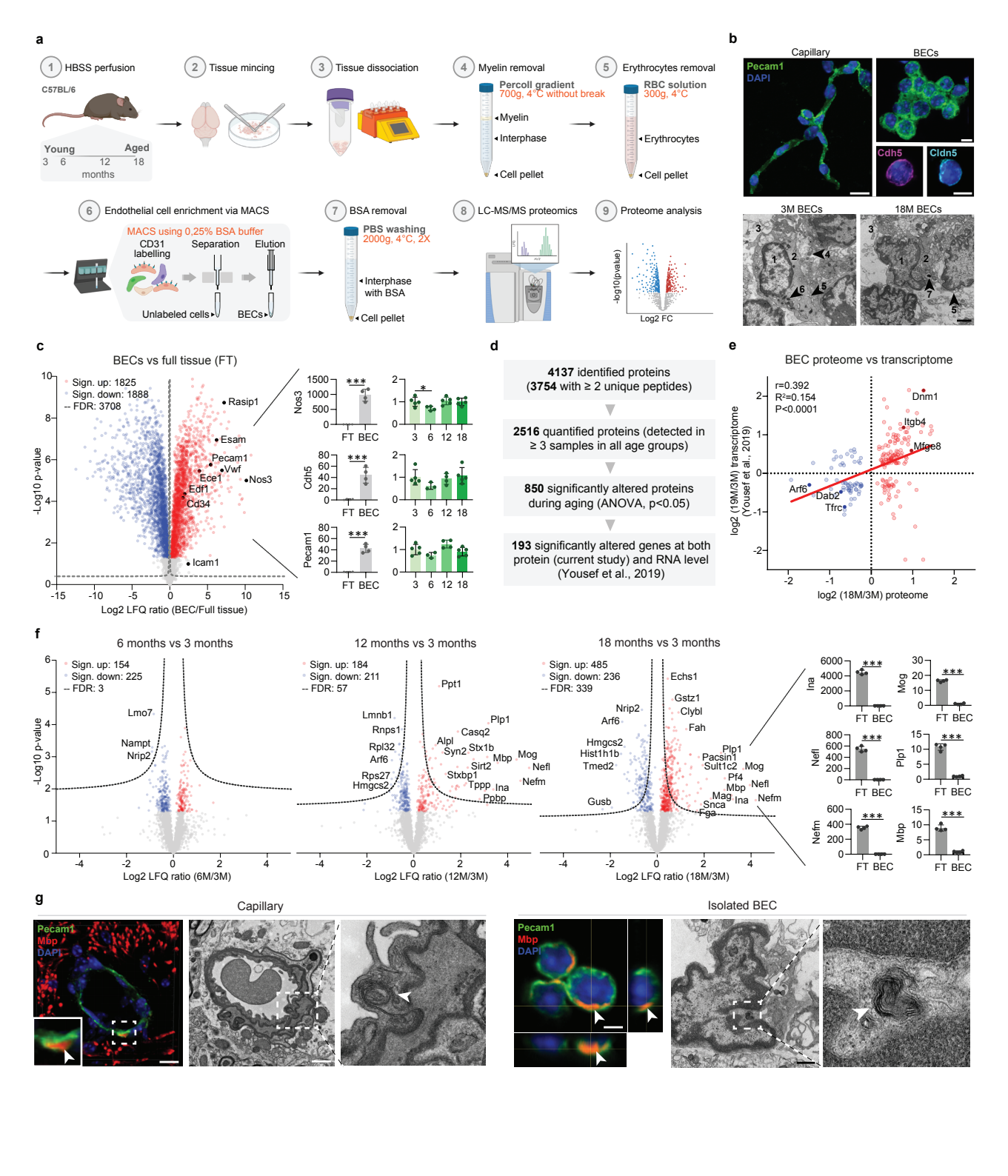
a
1 HBSS perfusion
C57BL/6
Young
Aged
3 6 12 18
months
2 Tissue mincing
3 Tissue dissociation
4 Myelin removal
Percoll gradient
700g, 4°C without break
Myelin
Interphase
Cell pellet
5 Erythrocytes removal
RBC solution
300g, 4°C
Erythrocytes
Cell pellet
6 Endothelial cell enrichment via MACS
MACS using 0,25% BSA buffer
CD31 labelling
Separation
Elution
Unlabeled cells
BECs
7 BSA removal
PBS washing
2000g, 4°C, 2X
Interphase with BSA
Cell pellet
8 LC-MS/MS proteomics
9 Proteome analysis
-log10(pvalue)
Log2 FC
b
Capillary
BECs
Pecam1
DAPI
Cdh5
Cldn5
3M BECs
18M BECs
c
BECs vs full tissue (FT)
Sign. up: 1825
Sign. down: 1888
-- FDR: 3708
Rasip1
Esam
Pecam1
Vwf
Ece1
Nos3
Edf1
Cd34
Icam1
-Log10 p-value
Log2 LFQ ratio (BEC/Full tissue)
Nos3
Cdh5
Pecam1
FT BEC
3 6 12 18
d
4137 identified proteins
(3754 with ≥ 2 unique peptides)
2516 quantified proteins (detected in ≥ 3 samples in all age groups)
850 significantly altered proteins during aging (ANOVA, p<0.05)
193 significantly altered genes at both protein (current study) and RNA level (Yousef et al., 2019)
e
BEC proteome vs transcriptome
r=0.392
R²=0.154
P<0.0001
Dnm1
Itgb4
Mfge8
Arf6
Dab2
Tfrc
log2 (19M/3M) transcriptome (Yousef et al., 2019)
log2 (18M/3M) proteome
f
6 months vs 3 months
Sign. up: 154
Sign. down: 225
-- FDR: 3
Lmo7
Nampt
Nrip2
12 months vs 3 months
Sign. up: 184
Sign. down: 211
-- FDR: 57
Ppt1
Lmnb1
Rnps1
Rpl32
Arf6
Rps27
Hmgcs2
Plp1
Casq2
Alpl
Syn2
Stx1b
Mbp
Mog
Sirt2
Nefl
Stxbp1
Tppp
Ina
Nefm
Ppbp
18 months vs 3 months
Sign. up: 485
Sign. down: 236
-- FDR: 339
Echs1
Gstz1
Clybl
Fah
Nrip2
Arf6
Hmgcs2
Hist1h1b
Tmed2
Gusb
Plp1
Pacsin1
Sult1c2
Mog
Pf4
Mbp
Nefl
Mag
Ina
Nefm
Snca
Fga
Log2 LFQ ratio (6M/3M)
Log2 LFQ ratio (12M/3M)
Log2 LFQ ratio (18M/3M)
Ina
Mog
Nefl
Plp1
Nefm
Mbp
FT BEC
g
Capillary
Isolated BEC
Pecam1
Mbp
DAPI


a
Clusters
1 2 3 4 5 6 7 8 9 10 11 12 13 14 15 16
All (count) 312 297 240 226 214 177 162 149 149 123 102 99 96 75 51 44
Significant (count) 119 83 112 100 81 63 70 55 41 26 17 28 13 17 19 6
Age related expression
Subcellular localization
Cytoplasm
Vesicle / Exosome
Cell / Adherent junction
Cytoskeleton
Plasma membrane
Endoplasmic reticulum
Ribosome
Nucleus
Mitochondrion
Myelin sheet
Biological processes
Protein catabolism
Cytoskeleton organization
Integrin-mediated signaling
Cell / cell-cell adhesion
Endocytosis
Translation
RNA splicing
Vesicle-mediated transport
Oxidation-reduction
Lipid metabolism
5-2 8-21 (p-value)
1.3 8 (enrichment)
b
Cluster 7
Cluster 3
Cluster 4
Cluster 8
Cluster 9
Cluster 2
protein expression
3
0
-3
3 6 12 18
age groups (months)
significant
identified
confidence interval
mean
c
Atp5a1 Gdpd1 Hint2 Htra2 Mif Pc Pdxdc1 Sel1l
Acaa1a Acaa2 Acadl Crat Decr1 Etfb Fasn Fdxr Gpd1 Ndufs6 Rdh5
Aass Acad10 Aco2 Aldh6a1 Aldh7a1 Asph Bckdhb Cbr3 Dlst Gfer Hk1 Idh2 L2hgdh Me2 Msrb2 Ndufa2 Ndufb5 Ppox Prdx5 Prodh Pycr2 Sucla2 Suclg1 Suclg2 Suox Uqcrh
6mo
12mo
18mo
Lipid metabolism (C4)
Lipid metabolism / Oxidation-reduction (C4)
Oxidation-reduction (C4)
Abce1 Eif3i Eif4e Iars Rpl10a Rpl18a Rpl19 Rpl24 Rpl34 Rpl6 Rpl8 Rps11 Rps13 Rps2 Rps3 Rps9
Ddx17 Ddx5 Hnrnph1 Nono Phf5a Prpf8 Rnps1 Sfpq Snrnp40 Snrpa Srsf1 Srsf2 Srsf7 Tra2b
Adam10 Ctnnd1 Itga1 Itga6 Itpr3 Pde2a Plcg1 Ppp2r2a Ptprm Snx1 Stat3 Tjp1 Tjp2 Tns1 Vamp3
Translation (C9)
RNA splicing (C3)
Cell adhesion (C2)
Akap12 Dbnl Dnm2 Flna Ilk Iqgap1 Lasp1 Map4 Myh9 Pls3 Pxn Sorbs3 Vcl
Clip1 Coro1b Dctn2 Ddah2 Dync1h1 Fgd5 Hook3 Nes Nos3 Stom
Arf6 Bcap31 Calr Canx Cltc Copa Ctsh Dab2 Hsp90ab1 Hspa4 Rab5c Sec61a1 Stx3 Tmed2 Tmed7 Tmem33 Vdac3
6
(fold change)
0.3
Cell adhesion / Cytoskeleton organization (C2)
Cytoskeleton organization (C2)
Vesicle-mediated transport (C3)

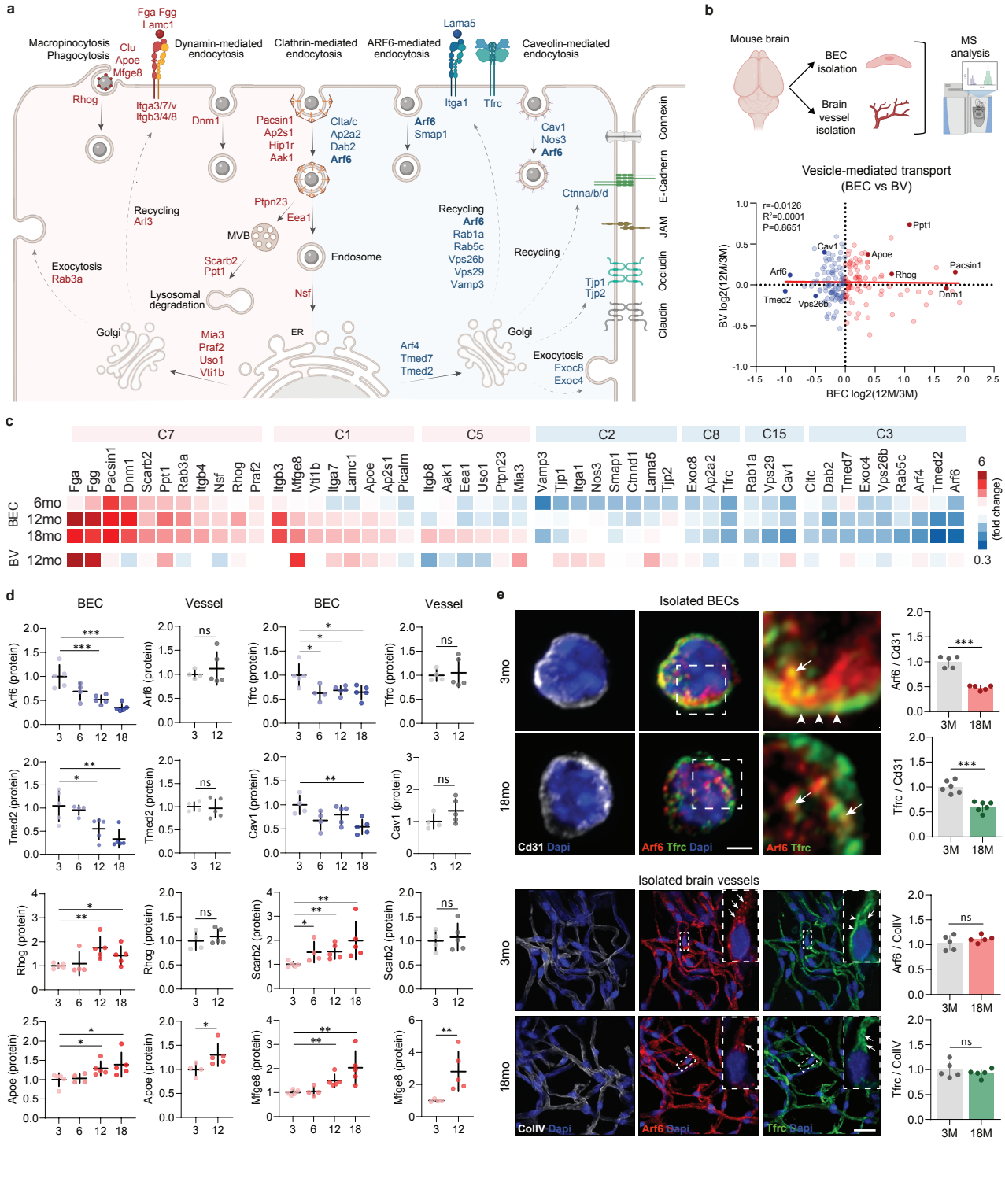
a
Macropinocytosis
Phagocytosis
Clu
Apoe
Mfge8
Fga Fgg
Lamc1
Dynamin-mediated endocytosis
Clathrin-mediated endocytosis
ARF6-mediated endocytosis
Lama5
Caveolin-mediated endocytosis
Rhog
Itga3/7/v
Itgb3/4/8
Dnm1
Pacsin1
Ap2s1
Hip1r
Aak1
Clta/c
Ap2a2
Dab2
Arf6
Itga1
Tfrc
Arf6
Smap1
Cav1
Nos3
Arf6
Connexin
E-Cadherin
JAM
Occludin
Claudin
Ctnna/b/d
Tjp1
Tjp2
Recycling
Arl3
Ptpn23
Eea1
MVB
Endosome
Scarb2
Ppt1
Lysosomal degradation
Nsf
Exocytosis
Rab3a
Recycling
Arf6
Rab1a
Rab5c
Vps26b
Vps29
Vamp3
Recycling
Golgi
Mia3
Praf2
Uso1
Vti1b
ER
Arf4
Tmed7
Tmed2
Golgi
Exocytosis
Exoc8
Exoc4
b
Mouse brain
BEC isolation
Brain vessel isolation
MS analysis
Vesicle-mediated transport (BEC vs BV)
r=-0.0126
R²=0.0001
P=0.8651
BV log2(12M/3M)
BEC log2(12M/3M)
Ppt1
Cav1
Apoe
Pacsin1
Arf6
Rhog
Tmed2
Vps26b
Dnm1
c
C7
C1
C5
C2
C8
C15
C3
Fga
Fgg
Pacsin1
Dnm1
Scarb2
Ppt1
Rab3a
Itgb4
Nsf
Rhog
Praf2
Itgb3
Mfge8
Vti1b
Itga7
Lamc1
Apoe
Ap2s1
Picalm
Itgb8
Aak1
Eea1
Uso1
Ptpn23
Mia3
Vamp3
Tjp1
Itga1
Nos3
Smap1
Ctnnd1
Lama5
Tjp2
Exoc8
Ap2a2
Tfrc
Rab1a
Vps29
Cav1
Cltc
Dab2
Tmed7
Exoc4
Vps26b
Rab5c
Arf4
Tmed2
Arf6
BEC
6mo
12mo
18mo
BV
12mo
6
(fold change)
0.3
d
BEC
Vessel
BEC
Vessel
Arf6 (protein)
Tfrc (protein)
Tmed2 (protein)
Cav1 (protein)
Rhog (protein)
Scarb2 (protein)
Apoe (protein)
Mfge8 (protein)
ns
e
Isolated BECs
3mo
18mo
Cd31 Dapi
Arf6 Tfrc Dapi
Arf6 Tfrc
Arf6 / Cd31
Tfrc / Cd31
3M
18M
Isolated brain vessels
3mo
18mo
CollV Dapi
Arf6 Dapi
Tfrc Dapi
Arf6 / CollV
Tfrc / CollV
3M
18M
ns

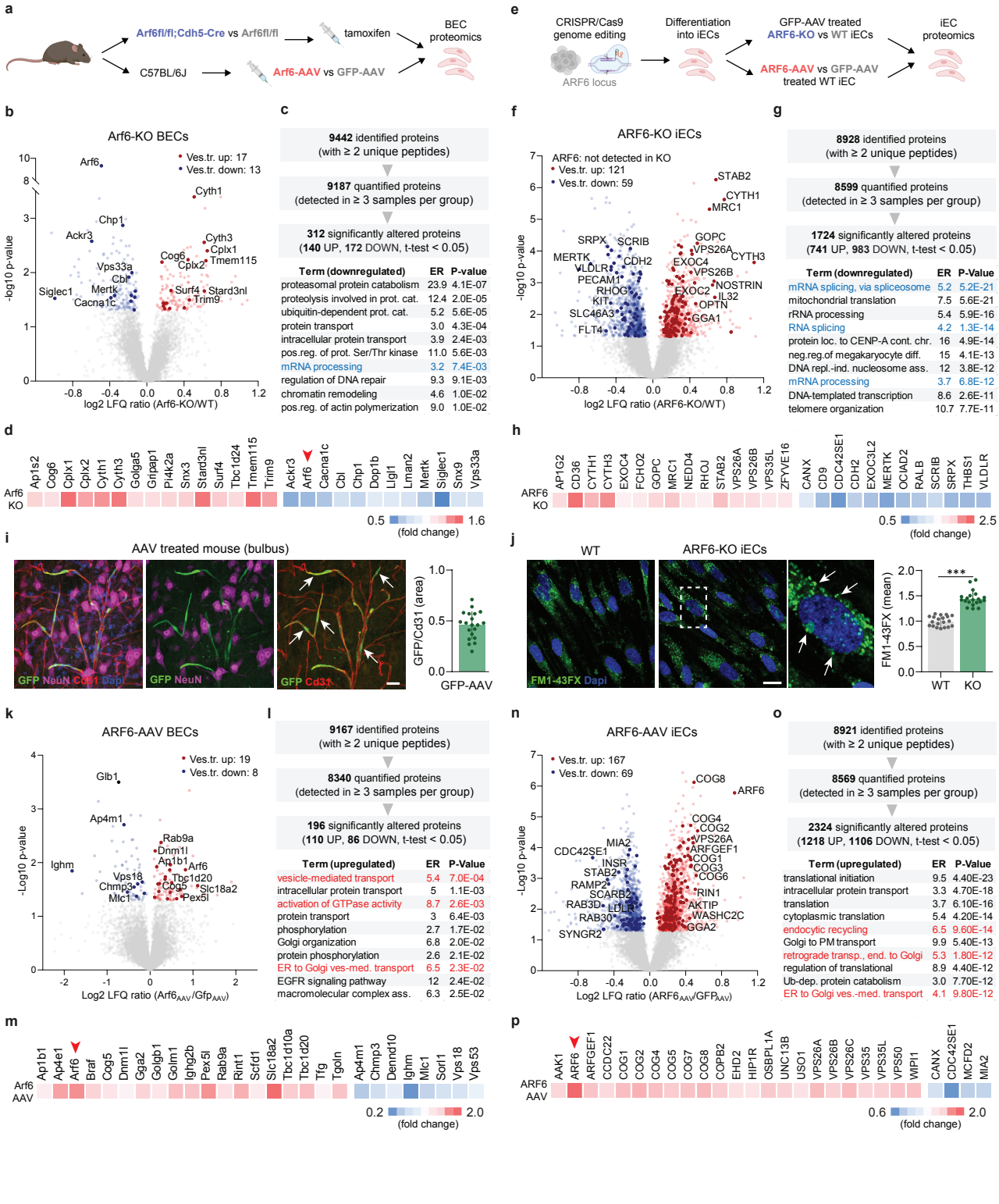
a
Arf6fl/fl;Cdh5-Cre vs Arf6fl/fl
tamoxifen
BEC proteomics
C57BL/6J
Arf6-AAV vs GFP-AAV
e
CRISPR/Cas9 genome editing
Differentiation into iECs
GFP-AAV treated ARF6-KO vs WT iECs
iEC proteomics
ARF6 locus
ARF6-AAV vs GFP-AAV treated WT iEC
b
Arf6-KO BECs
Ves.tr. up: 17
Ves.tr. down: 13
-log10 p-value
log2 LFQ ratio (Arf6-KO/WT)
c
9442 identified proteins (with ≥ 2 unique peptides)
9187 quantified proteins (detected in ≥ 3 samples per group)
312 significantly altered proteins (140 UP, 172 DOWN, t-test < 0.05)
Term (downregulated) | ER | P-value
proteasomal protein catabolism | 23.9 | 4.1E-07
proteolysis involved in prot. cat. | 12.4 | 2.0E-05
ubiquitin-dependent prot. cat. | 5.2 | 5.6E-05
protein transport | 3.0 | 4.3E-04
intracellular protein transport | 3.9 | 2.4E-03
pos.reg. of prot. Ser/Thr kinase | 11.0 | 5.6E-03
mRNA processing | 3.2 | 7.4E-03
regulation of DNA repair | 9.3 | 9.1E-03
chromatin remodeling | 4.6 | 1.0E-02
pos.reg. of actin polymerization | 9.0 | 1.0E-02
f
ARF6-KO iECs
ARF6: not detected in KO
Ves.tr. up: 121
Ves.tr. down: 59
-log10 p-value
log2 LFQ ratio (ARF6-KO/WT)
g
8928 identified proteins (with ≥ 2 unique peptides)
8599 quantified proteins (detected in ≥ 3 samples per group)
1724 significantly altered proteins (741 UP, 983 DOWN, t-test < 0.05)
Term (downregulated) | ER | P-Value
mRNA splicing, via spliceosome | 5.2 | 5.2E-21
mitochondrial translation | 7.5 | 5.6E-21
rRNA processing | 5.4 | 5.9E-16
RNA splicing | 4.2 | 1.3E-14
protein loc. to CENP-A cont. chr. | 16 | 4.9E-14
neg.reg.of megakaryocyte diff. | 15 | 4.1E-13
DNA repl.-ind. nucleosome ass. | 12 | 3.8E-12
mRNA processing | 3.7 | 6.8E-12
DNA-templated transcription | 8.6 | 2.6E-11
telomere organization | 10.7 | 7.7E-11
d
Arf6 KO
0.5
1.6
(fold change)
h
ARF6 KO
0.5
2.5
(fold change)
i
AAV treated mouse (bulbus)
GFP NeuN Cd31 Dapi
GFP NeuN
GFP Cd31
GFP/Cd31 (area)
GFP-AAV
j
WT
ARF6-KO iECs
FM1-43FX Dapi
FM1-43FX (mean)
***
WT
KO
k
ARF6-AAV BECs
Ves.tr. up: 19
Ves.tr. down: 8
-Log10 p-value
Log2 LFQ ratio (Arf6AAV/GfpAAV)
l
9167 identified proteins (with ≥ 2 unique peptides)
8340 quantified proteins (detected in ≥ 3 samples per group)
196 significantly altered proteins (110 UP, 86 DOWN, t-test < 0.05)
Term (upregulated) | ER | P-Value
vesicle-mediated transport | 5.4 | 7.0E-04
intracellular protein transport | 5 | 1.1E-03
activation of GTPase activity | 8.7 | 2.6E-03
protein transport | 3 | 6.4E-03
phosphorylation | 2.7 | 1.7E-02
Golgi organization | 6.8 | 2.0E-02
protein phosphorylation | 2.6 | 2.1E-02
ER to Golgi ves-med. transport | 6.5 | 2.3E-02
EGFR signaling pathway | 12 | 2.4E-02
macromolecular complex ass. | 6.3 | 2.5E-02
n
ARF6-AAV iECs
Ves.tr. up: 167
Ves.tr. down: 69
-Log10 p-value
Log2 LFQ ratio (ARF6AAV/GFPAAV)
o
8921 identified proteins (with ≥ 2 unique peptides)
8569 quantified proteins (detected in ≥ 3 samples per group)
2324 significantly altered proteins (1218 UP, 1106 DOWN, t-test < 0.05)
Term (upregulated) | ER | P-Value
translational initiation | 9.5 | 4.40E-23
intracellular protein transport | 3.3 | 4.70E-18
translation | 3.7 | 6.10E-16
cytoplasmic translation | 5.4 | 4.20E-14
endocytic recycling | 6.5 | 9.60E-14
Golgi to PM transport | 9.9 | 5.40E-13
retrograde transp., end. to Golgi | 5.3 | 1.80E-12
regulation of translational | 8.9 | 4.40E-12
Ub-dep. protein catabolism | 3.0 | 7.70E-12
ER to Golgi ves.-med. transport | 4.1 | 9.80E-12
m
Arf6 AAV
0.2
2.0
(fold change)
p
ARF6 AAV
0.6
2.0
(fold change)

a

Disease	Count	ER	FDR
Metabolism, Inborn Errors	60	3.10	9.0E-12
Stress	77	2.57	1.8E-11
Shock	52	3.11	2.0E-10
Genetic Diseases, Inborn	40	3.54	1.5E-09
Neurodegenerative Diseases	60	2.66	1.7E-09
Mitochondrial Diseases	52	2.81	5.8E-09
Brain Diseases	59	2.53	1.6E-08
Central Nervous System Diseases	59	2.50	2.1E-08
Brain Diseases, Metabolic	31	3.81	3.2E-08
Parkinson Disease	34	3.39	5.7E-07
FTLD	17	5.25	3.1E-06
Protein deficiency disease	40	2.65	3.8E-06
Metabolic Diseases	67	2.00	7.5E-06
Parkinsonian Disorders	27	3.26	1.1E-05
Anemia, Diamond-Blackfan	10	8.07	2.7E-05
FTDP-17	15	4.77	6.0E-05
Movement Disorders	33	2.60	7.2E-05
Protein Deficiency	49	2.08	1.3E-04
Cholera	15	4.37	1.5E-04
Wiskott-Aldrich Syndrome	19	3.59	1.5E-04
Dementia	30	2.51	4.0E-04
Dementia, Vascular	9	5.83	5.5E-04
Basal Ganglia Diseases	27	2.54	8.9E-04
Acidosis	20	2.92	1.6E-03
Alzheimer Disease	30	2.40	2.8E-03

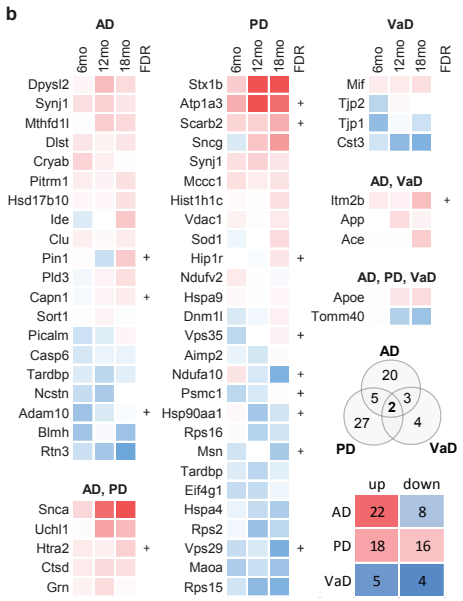

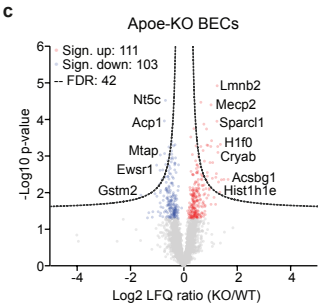

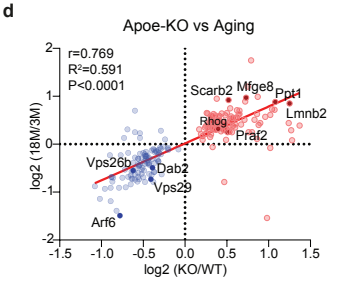

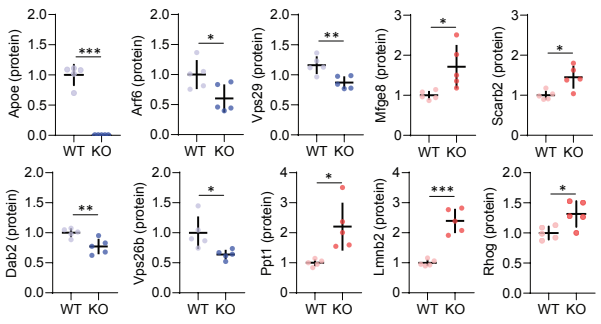

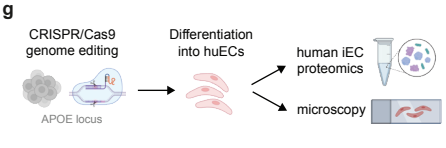

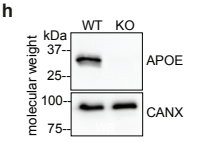

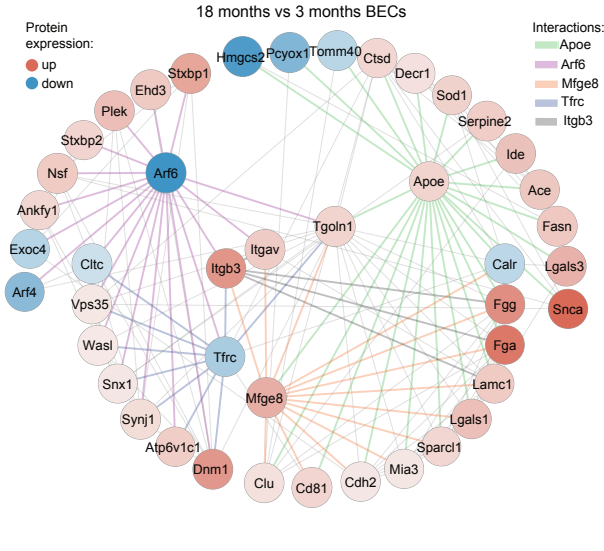

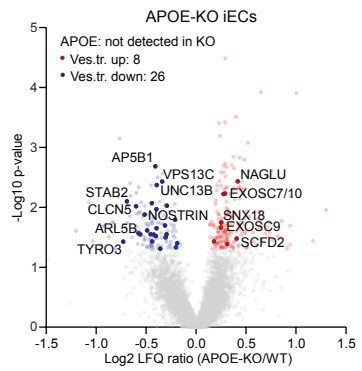

j

8897 identified proteins
(with ≥ 2 unique peptide)

8446 quantified proteins
(detected in ≥ 3 samples per group)

326 significantly altered proteins
(**196** UP, **130** DOWN, t-test < 0.05)

Term (downregulated)	ER	P-value
cytoplasmic translation	14.2	9.5E-06
vesicle-mediated transport	6.9	4.6E-05
reg. of transcription factor activ.	29.2	3.3E-04
translation	5.8	1.3E-03
intracellular signal transduction	3.7	3.1E-03
cell. resp. to interferon-gamma	7.5	1.6E-02
protein phosphorylation	3.0	1.7E-02
axon guidance	4.8	2.0E-02
autophagosome maturation	13.0	2.2E-02
vesicle fusion	13.0	2.2E-02

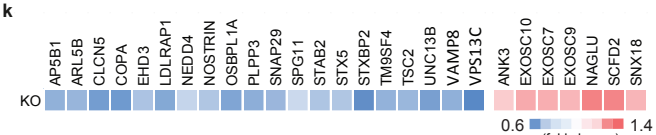

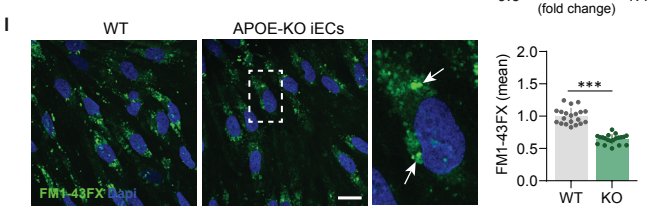

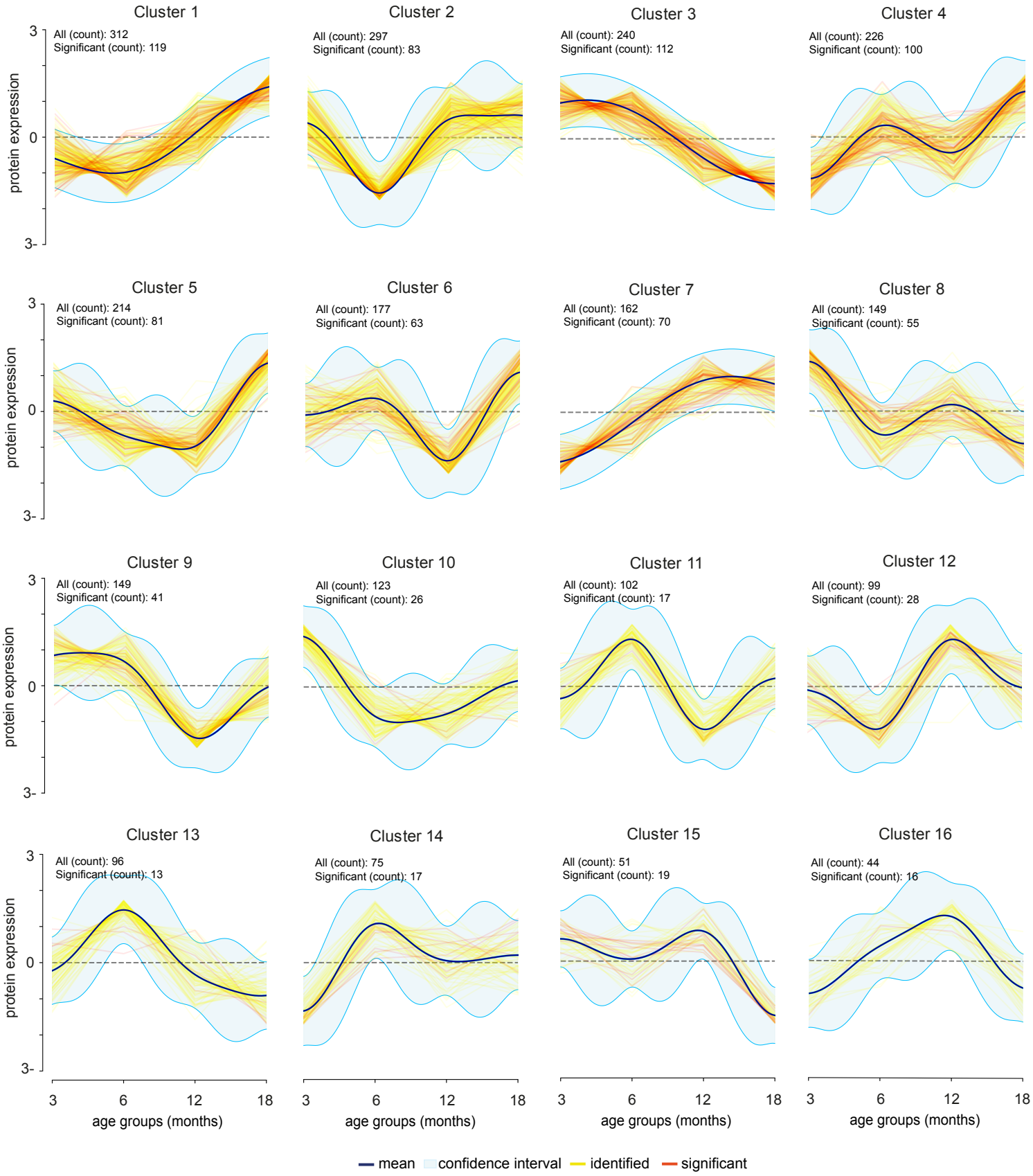
Cluster 1
All (count): 312
Significant (count): 119
Cluster 2
All (count): 297
Significant (count): 83
Cluster 3
All (count): 240
Significant (count): 112
Cluster 4
All (count): 226
Significant (count): 100
Cluster 5
All (count): 214
Significant (count): 81
Cluster 6
All (count): 177
Significant (count): 63
Cluster 7
All (count): 162
Significant (count): 70
Cluster 8
All (count): 149
Significant (count): 55
Cluster 9
All (count): 149
Significant (count): 41
Cluster 10
All (count): 123
Significant (count): 26
Cluster 11
All (count): 102
Significant (count): 17
Cluster 12
All (count): 99
Significant (count): 28
Cluster 13
All (count): 96
Significant (count): 13
Cluster 14
All (count): 75
Significant (count): 17
Cluster 15
All (count): 51
Significant (count): 19
Cluster 16
All (count): 44
Significant (count): 16
protein expression
3
0
3-
3
6
12
18
age groups (months)
mean
confidence interval
identified
significant

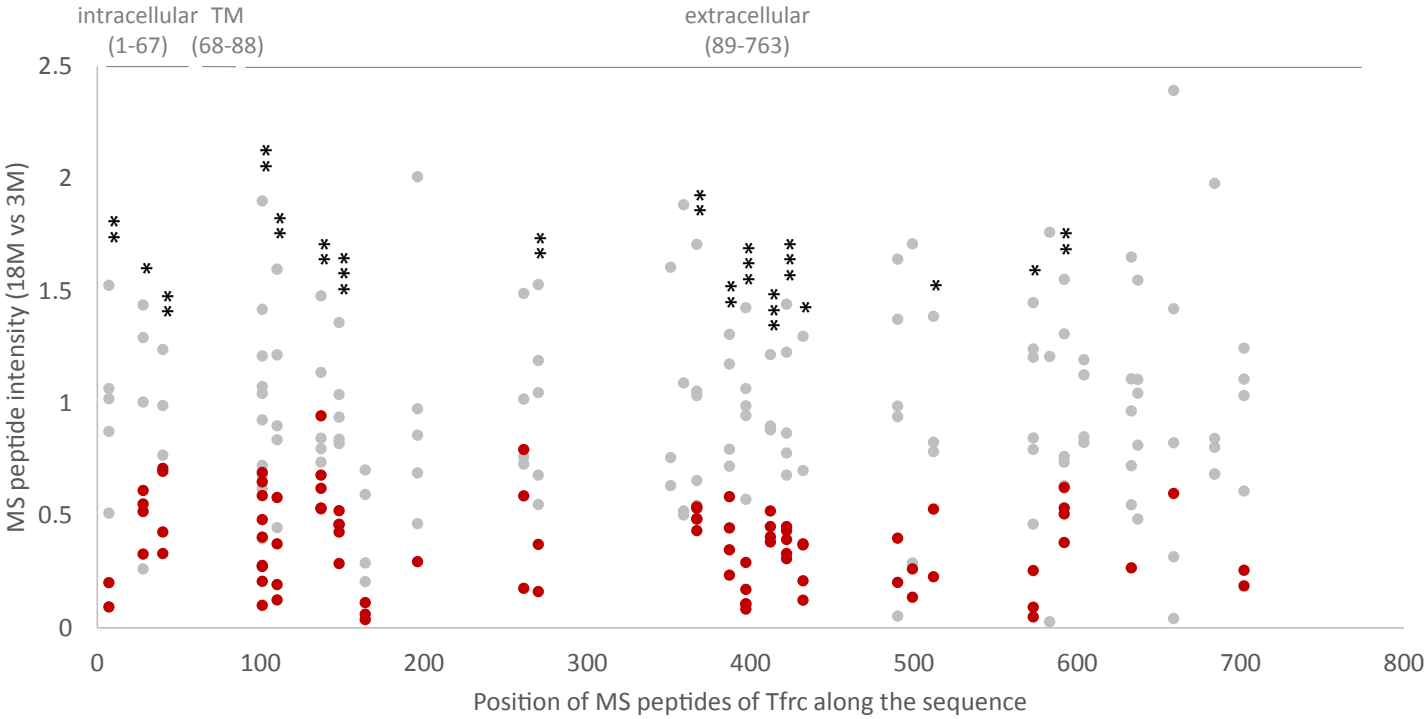
intracellular
(1-67)
TM
(68-88)
extracellular
(89-763)
MS peptide intensity (18M vs 3M)
2.5
2
1.5
1
0.5
0
0
100
200
300
400
500
600
700
800
Position of MS peptides of Tfrc along the sequence

A

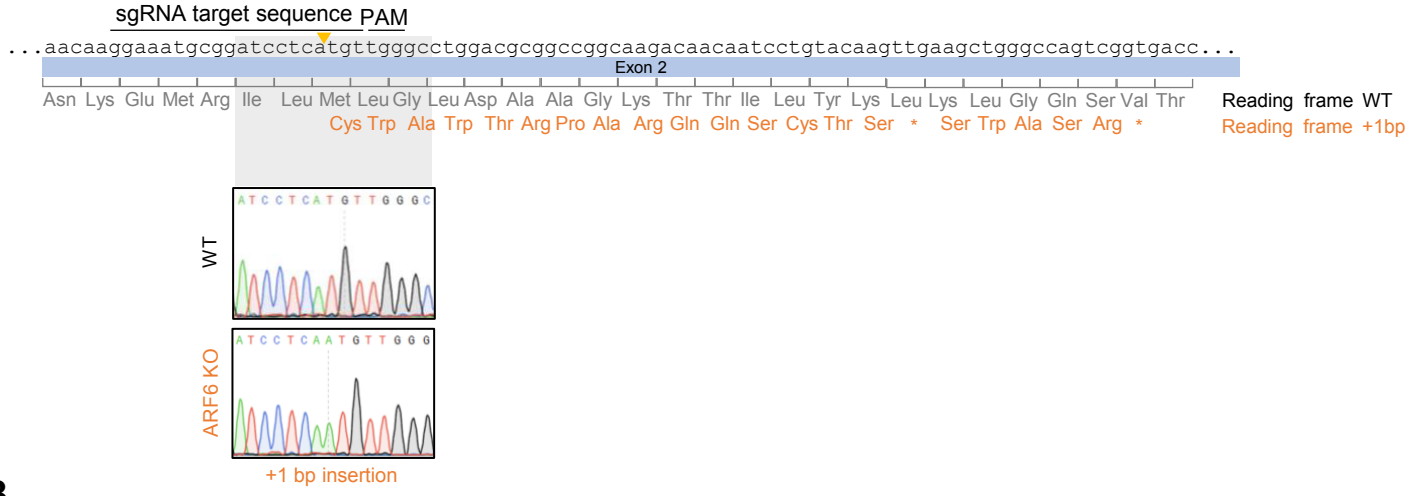

B

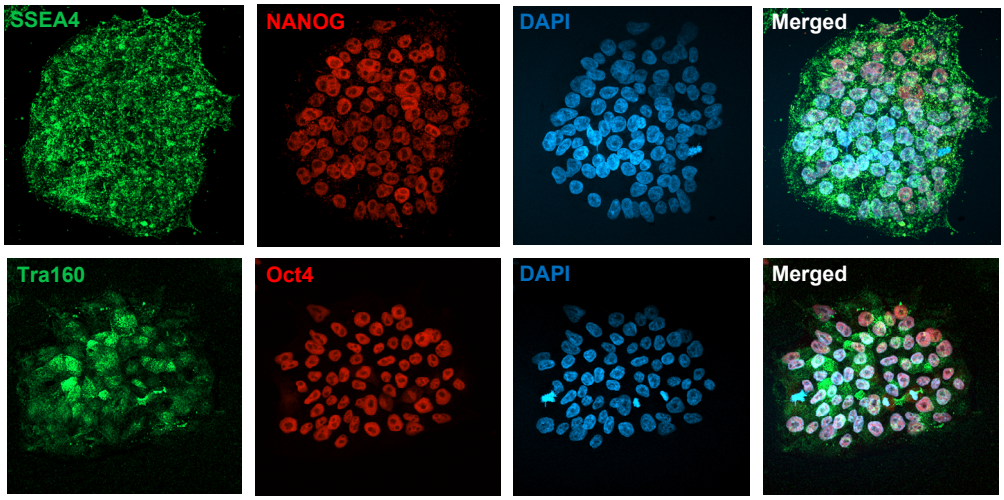

C

Gene	ID	Sequence	Mismatch position	Mismatch Count	MIT score	CFD score	Location	Locus description	Indels detected
ARF6	gRNA	GGAAATGCGGATCCTCATGTTGG	Target		-	-	-	-	-
ARF6	CFD OT 1	GGAAAAATGTATCCTCATGTAGG	.....***.*.....	4	0.496624	0.616146	8:134804959:134805481:-1	intergenic:MIR30D-AC083843.2	None
ARF6	CFD OT 2	TGAAATGTAGACCCTCATGTTGG	*.....**..*.....	4	0.430092	0.532895	13:36733486:36734008:1	intergenic:AL136160.1-RFXAP	None
ARF6	CFD OT 3	AGAAATGTGGAACTTCATGTGGG	*.....*...*.*.....	4	0.110194	0.462	4:78874823:78875345:1	intron:BMP2K	None
ARF6	CFD OT 4	GAAAATGCAGATCCTAATTTCGG	.*.....*.....*..*.	4	0.052415	0.362637	20:5032709:5033231:1	intergenic:SLC23A2-RP5-1116H23.6	None
ARF6	CFD OT 5	GGAAATGTTGATCTTAATGTGGG	.....**....*.*....	4	0.021373	0.342222	13:58747536:58748058:-1	intergenic:RNY4P29-AL359262.1	None
ARF6	MIT OT 1	AGTAGTGAGGATCCTCATGTTGG	*.*.*..*.....	4	1.345833	0.297318	5:92369914:92370436:-1	intergenic:RP11-348J24.1-RP11-348J24.2	None
ARF6	MIT OT 2	GGGAATCGGAATCCTCATGTGGG	..*...**.*.....	4	0.846587	0.252083	1:166974117:166974639:1	intron:ILDR2	None
ARF6	MIT OT 3	AGAGATGGGGTTCCTCATGTTGG	*..*...*..*.....	4	0.794051	0.111264	2:233186656:233187178:1	intron:INPP5D	None
ARF6	MIT OT 4	GAAGATGTGGATCCTCATGGTGG	.*.*...*.....*	4	0.697447	0.08166	6:27107660:27108182:1	intergenic:TRI-TAT2-2-RNU2-62P	None
ARF6	MIT OT 5	GTAAATGAGAATCCTCATGAGGG	.*.....*.*.....*	4	0.642349	0.217159	6:5830623:5831145:-1	intergenic:FARS2-RP3-380B8.4	None

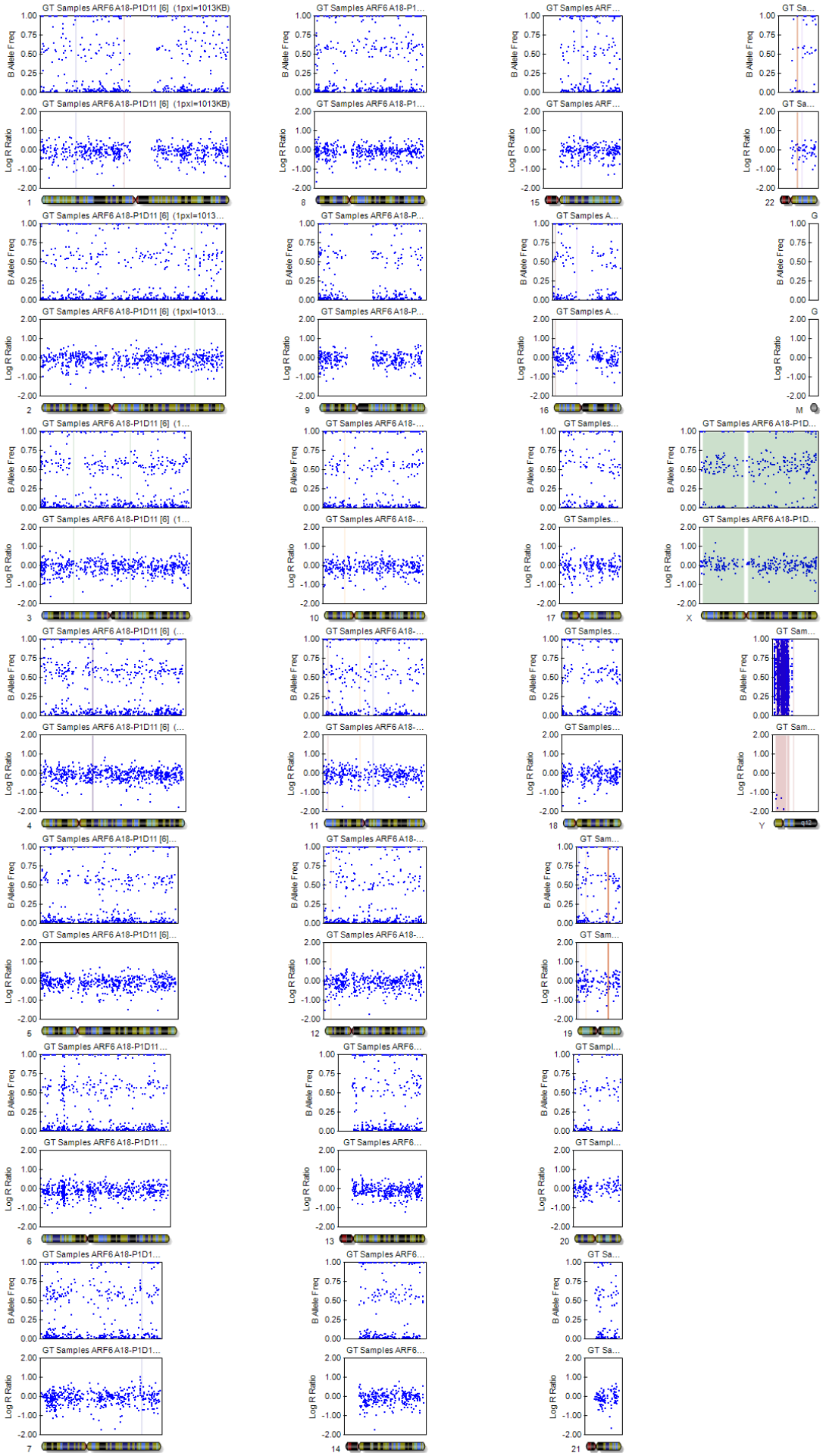
GT Samples ARF6 A18-P1D11 [6] (1pxl=1013KB)
B Allele Freq
Log R Ratio
1
8
15
22
2
9
16
M
3
10
17
X
4
11
18
Y
5
12
19
6
13
20
7
14
21

A

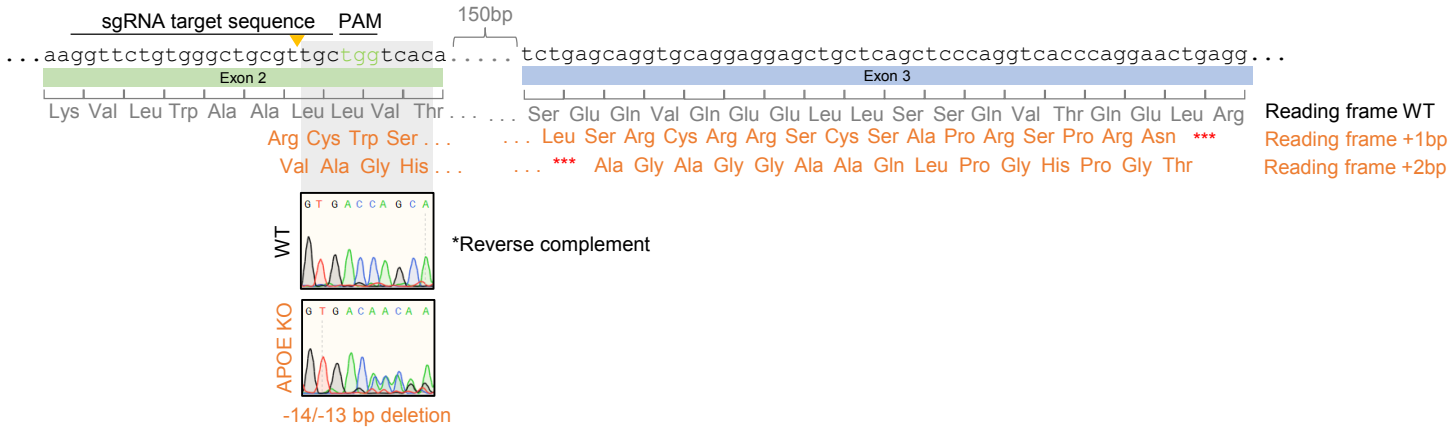

B

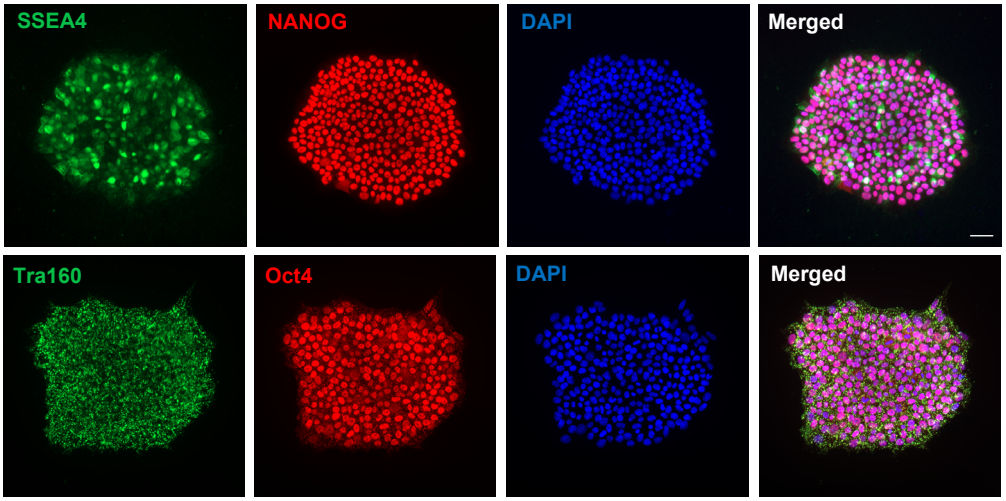

C

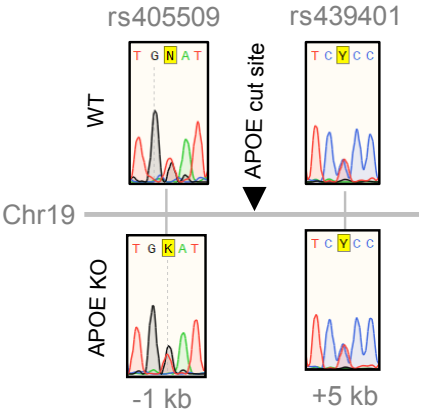

D

Gene	ID	Sequence	Mismatch Position	Mismatch Count	MIT Score	CFD Score	Location	Location Description	Indels detected
APOE	gRNA	GGTTCTGTGGGCTGCGTTGCTGG	Target						
APOE	CFD OT1	AGTTCTGTGGACTCCATTGCAGG	*.....*..*.*....	4	0,023	0,386	4:152072154:152072676:-1	intergenic:RNA5SP169-RP11-18H21.1	None
APOE	CFD OT2	GGTTCTGGGGAATGCGTTTCTGG	.....*..**.....*.	4	0,123	0,349	13:114048991:114049513:-1	intron:RASA3	None
APOE	CFD OT3	AGTTCAGTTGGCAGCGTTGCAGG	*....*..*...*.....	4	0,215	0,288	14:101784777:101785299:1	intron:PPP2R5C	None
APOE	MIT OT1	GATTCTGTGGGCTGCGTGGCAGG	.*.............*..	2	3,003	0,282	11:116563492:116564014:1	intergenic:AP001891.1-AP000770.2	None
APOE	MIT OT2	GGTTCTTAGAGCTGCGTTGCTGG	.....**.*.....	3	1,459	0,427	12:47887516:47888038:-1	intergenic:RP11-89H19.1/VDR-RP11-89H19.1	None
APOE	MIT OT3	CGTTCTGAGGGCTGCCTTGCAGG	*.....*.....*....	3	0,542	0	2:46084987:46085509:1	intergenic:AC017006.2-PRKCE	None
APOE	MIT OT4	GGATCTGAGAGCAGCGTTGCTGG	..*....*.*..*.....	4	0,503	0,369	5:54520000:54520522:1	intron:SNX18	None
APOE	MIT OT5	GGTTCTGTGCTCTGCGGTGCTGG	.....**.....*...	3	0,501	0,018	4:148066707:148067229:1	intron:ARHGAP10	None

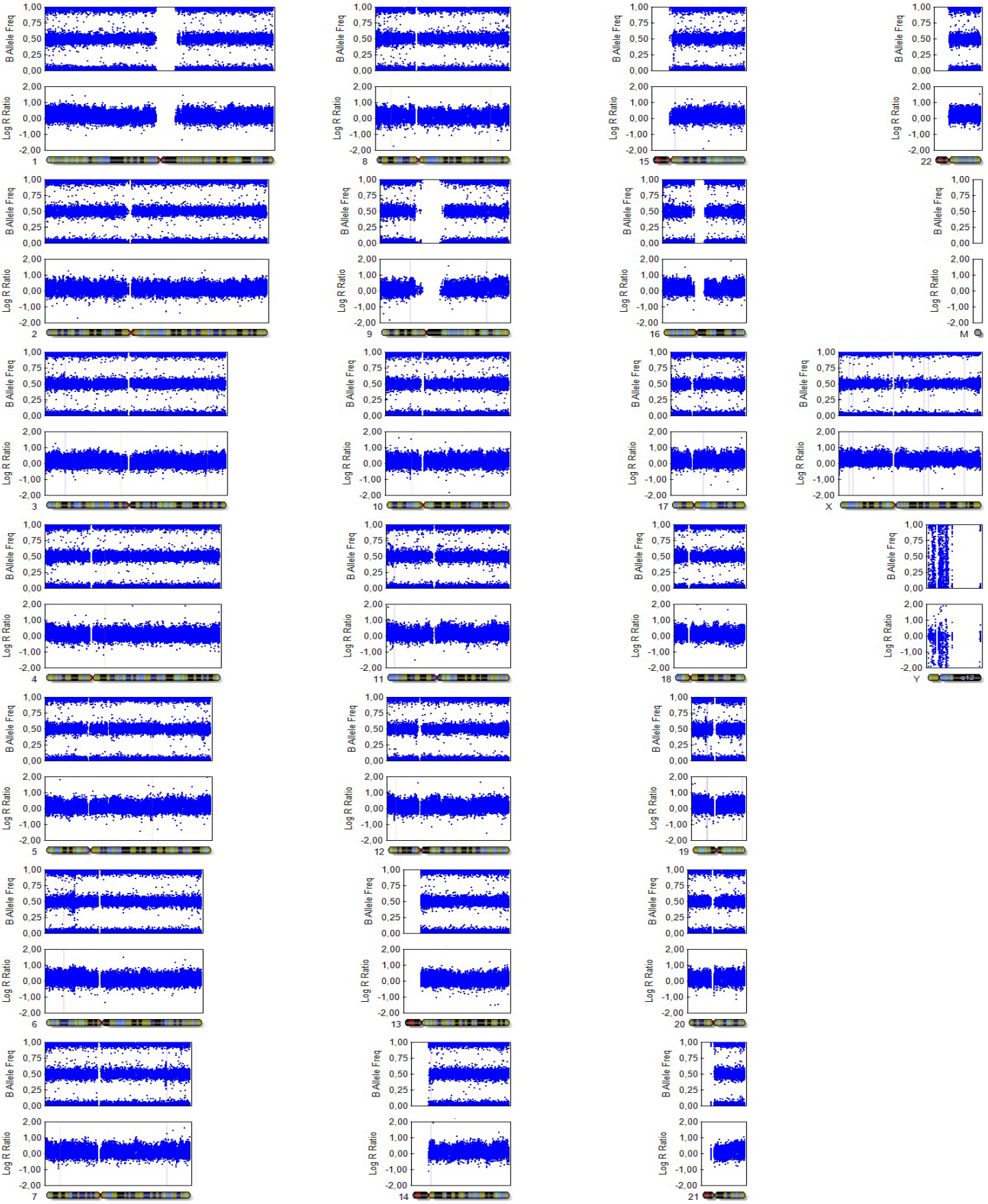
B Allele Freq
1,00
0,75
0,50
0,25
0,00
Log R Ratio
2,00
1,00
0,00
-1,00
-2,00
1
8
15
22
2
9
16
M
3
10
17
X
4
11
18
Y
5
12
19
6
13
20
7
14
21